DIPLOMARBEIT

DIPLOMA-THESIS

Numerical investigation of onset of brittle failure in CLT plates

ausgeführt zum Zwecke der Erlangung des
akademischen Grades eines Diplom-Ingenieurs

unter der Leitung von

Ass.-Prof. Dipl.-Ing. Dr. techn. **Karin Hofstetter**
E 202
Institut für Mechanik der Werkstoffe und Strukturen
Technische Universität Wien

eingereicht an der Technischen Universität Wien
Fakultät für Bauingenieurwesen

von

Daniel Schlattinger

Matr.-Nr.: 0226622
Naflastraße 58
A - 6800 Feldkirch

Wien, Juni 2011

Gewidmet meinen Großeltern Frieda und Franz

Abstract

This thesis deals with the mechanical behavior of 'Cross Laminated Timber (CLT)' plates, which is a well-established high-performance wood product used for modern domestic architecture as well as in structural engineering. Only recently, building regulations have been changed to allow application of wooden load-bearing components in multi-storied houses. CLT is playing an important role there. Though, currently available material models cannot capture the distinctive mechanical behavior of this shear compliant laminate and its plate-specific load transfer. Commonly, CLT is assessed by simplifying design approaches based on beam-theory. Under application of the Finite Element Method (FEM), an alternative and more precise analysis of the mechanical behavior is possible.

The main task of this thesis was to develop a simulation tool generating a FE model of a 3-layered quadratic CLT plate, where in particular a suitable description of the fracture behavior under tensile load should be integrated. When building the individual layers in the model of CLT, randomly distributed board lengths as well as randomly distributed densities and knot contents (in terms of KAR-values) are taken into consideration. The simulation-program, defining the model for the FE analysis with the commercial FE package *Abaqus* ^{TM}, is written in *Matlab* ^{TM}. It generates the geometry sections of the CLT plate as well as locally varying stiffness and strength values. The latter are determined from local densities and KAR-values by means of micromechanical models, developed at the Institute for Mechanics of Materials and Structures. Emphasis was placed on the ability of the simulation program to generate matched model definitions with different mesh densities, in order to investigate the influence of the chosen mesh on the simulation results.

The results of computations performed on a generated sample plate are qualitatively discussed. Furthermore, the effect of crack formation between the lamellae of a CLT plate is investigated.

Kurzfassung

Diese Arbeit befasst sich mit der Untersuchung des Materialverhaltens von Brettsperrholz-Platten (englisch 'Cross Laminated Timber' – CLT). CLT hat sich als gängiger Holzwerkstoff sowohl im Wohnbau als auch im modernen konstruktiven Ingenieurholzbau etabliert. Um moderne Holzwerkstoffe entsprechend ihrer Eignung einsetzen zu können, wurden Normen und Verordnungen für das Bauwesen dahingehend adaptiert, dass nun auch die Konstruktion mehrgeschossiger Gebäude mit einer tragende Struktur aus Holzwerkstoffen möglich ist. Und CLT ist ein gewichtiger Vertreter in der Familie von konstruktiven Holzwerkstoffen. Jedoch gibt es derzeit noch kein adäquates mechanischen Materialmodell für CLT, was einer

Ausnutzung der gesamten Leistungsfähigkeit dieses flächigen Holzwerkstoffes entgegensteht. CLT ist charakterisiert durch die inhomogene und anisotrope Materialstruktur des Grundwerkstoffes Holz auf der einen Seite, und die dem spezifischen Aufbau, mit aus 90° gegeneinander gedrehten Brettlagen, geschuldeten Eigenschaften. Diese äußern sich in einer hohen Schubnachgiebigkeit der mittleren Schichten und den daraus resultierenden spezifischen Lastverhältnissen innerhalb der Platten. Derzeit werden für die Bemessung von CLT vereinfachende Rechenmodelle angewandt, die überwiegend auf der Stabtheorie basieren. Jedoch ist in Anwendung der Finiten Elemente Methode (FEM) eine umfangreichere und präzisere mechanische Berechnung auch bei Holzwerkstoffen möglich. Die Modellbildung gestaltet sich hingegen komplexer als zum Beispiel im Stahl- oder Betonbau, wo FEM längst eine Anwendung in der täglichen Baupraxis erfahren hat.

Die wesentliche Aufgabe der hier präsentierten Arbeit bestand darin, ein Simulations-programm zur Generierung einer quadratischen CLT-Platte zu entwickeln. Im Besonderen sollte ein Modell etabliert werden, welches die Rissbildung zwischen den einzelnen Lamellen in der Zugzone bei hoher Biegebeanspruchung mechanisch abbilden kann. Um ein werkstoffmechanisches Modell von CLT zu erstellen, ist es zuallererst nötig den Aufbau der einzelnen Schichten aus Schnitthölzern zu betrachten. In diesen Schichten sind die Längen der einzelnen Schnittholzabschnitte bedingt durch den Herstellungsprozess zufallsverteilt; ebenso unterliegen die Rohdichten und der abmindernde Einfluss von Ästen einer statistischen Verteilung. Bei der Erstellung des FE-Modells werden diese charakteristischen Verteilungen berücksichtigt, in dem den in geometrische Einheiten aufgeteilten Modell jeweils verschiedene Steifigkeits- und Festigkeitswerte zugewiesen werden. Letztere werden in Anwendung eines mikromechanischen Modells (entwickelt am Institut für Mechanik der Werkstoffe und Strukturen) aus der Rohdichte und dem KAR-Wert, welcher den Einfluss der Ästigkeit beschreibt, ermittelt. Die FE-Berechnungen sowie die mechanische Auswertungen erfolgen mit dem kommerziellen Programm *Abaqus* ^{TM}, das Simulationsprogramm wurde in *Matlab* ^{TM} erstellt. Bei der Festlegung der Spezifikationen des Simulationsprogramms wurde darauf geachtet, dass bei der Generierung von CLT-Platten die Feinheit des FE-Netzes aller Modellabschnitte parametergesteuert definiert werden kann, um so den Einfluss dieser Feinheit bei der mechanischen Analyse des Modells untersuchen zu können.

Die Ergebnisse der Berechnungen werden am Ende der Arbeit anhand einer repräsentativen Platte qualitativ ausgewertet. Ein Schwerpunkt der Analyse lag dabei auf der Untersuchung des mechanischen Einflusses der Riss-bildung auf das Gesamtsystem der Platte.

Contents

Chapter 1

Basic concept

1.1 Motivation

Cross Laminated Timber (CLT, ger. «Brettsperrholz») is a well-established high-performance wood product, and it enjoys great popularity in modern domestic architecture as well as in structural engineering. Currently, with the simplifying design approaches based on beam-theory, the distinctive mechanical characteristics of CLT, namely two-dimensional load transfer, multi-layer assembly, very high shear compliance of thick cross-lying layers, and anisotropy of the laminae, cannot be captured completely. Under application of the Finite Element Method (FEM), an alternative and more precise analysis of the mechanical behavior is possible. Based on former work at the Institute for Mechanics of Materials and Structures (IMWS), this thesis is a specific enhancement of an already existing model for CLT [Radecki-Pawlik, 2009]. The mechanic behavior of a quadratic CLT-Plate under uniformly distributed loading condition is in the main focus of this thesis. In particular a suitable description of the fracture behavior under tensile load is integrated.

Due to the pronounced anisotropy of the basic material wood as well as the characteristic assembling of CLT, the material behavior of CLT is studied by means of representative model sections, denoted as «CLT-Plates» in the following, which constitute the basis for the subsequent simulation. In relation to the structure of the calculation model, this thesis is organized in two parts: On the one hand, «simulation-program» generates adequate workpieces, on the other hand the «FE-program» performs the computations and is finally used for investigation of the CLT-Plates. The simulation-program is written in *Matlab* ^{TM} and defines parameters controlling the geometry of the CLT-plates as well as the load situation. Moreover, it specifies appropriate material parameters for the section-divided CLT-Plate. Applying the FE-program (*Abaqus* ^{TM}) the approximate solution of the displacement and stress-state of the CLT-Plate is determined. Compared to the mentioned former work, «cohesive-elements» were embedded in the tension-field of theplate. By means of these elements, the fracture behavior of wood under tension-load should be described.

1.2 Previous work

In timber-frame constructions, glulam beams are mainly strained in one direction. Therefore, one-dimensional beam theories are used for their static analysis. Though, by means of beam theories, mechanical characteristics of CLT cannot be represented sufficiently. Nowadays, use of the FEM is a standard design approach in concrete constructions to use the FE-method for determining the dimensions of plates. For a more efficient use of plate-like engineered wood products, the application of plate theories will be required.

Several studies have dealt with analytic calculations for laminated timber. At the IMWS, Stürzenbecher [Stürzenbecher, 2010] investigated and compared various common and advanced plate theories in relation to their accuracy as well as to their possible fields of application. Using a simply supported quadratic plate as example, he assessed classical plate theory as reference and various advanced plate theories (e.g. Murakami's Zig-Zag plate theory, Ren's Plate Theory), followed by an evaluation of the exact analytical solution derived by Pagano [Pagano, 1970]. The investigations resulted in the conclusion, that only Ren's Plate Theory approximates the exact solution sufficiently well. All the other theories are not capable to describe the characteristic mechanical behavior of CLT.

Radecki [Radecki-Pawlik, 2009] compared selected analytic exact results from the thesis of Stürzenbecher with numeric calculations, carried out by means of the FEM. The focus of his thesis lies on the investigation of normal and shear stresses at significant points of the plate. Their calculations were based on an elastic-plastic material behavior in the compression field of the CLT-Plate. Based on a comparison of the obtained load-displacement diagram with that of the reference-plate, which is calculated with ideal-elastic behavior, the elastic limit of the plate is calculated. In the present thesis, the simulation model by Radecki is extended by a fracture mechanical approach for wood under tension load. For the implementation of fracture mechanical material behavior, «cohesive-elements» were embedded in the FE-calculation. Also a parameter-controlled mesh-design is established, what enables a direct comparison of a coarse and a fine discretization level at otherwise identical geometry and material parameters.

1.3 Structure

The thesis is organized in four chapters. After the introductory chapter the basic mechanic constitutive equations are presented in Chapter 2. Furthermore regression equations for the determination of elastic parameters and strength values from the technological parameters density ρ and moisture content u in by means of a micromechanical model are explained. The influence of knots on the mechanical

properties is discussed thereafter as well as distribution functions for technological parameters and the knot content. To assign technological parameters to the material sections, the plate is divided in, distribution funcionts are presented. As completion of the theoretical background, the assembly of CLT and the distinctive approach for the modeling process as well as the used material models are presented. Chapter 3 describes the concept of the simulation program. As starting section, the ability of the simulation program is presented by means of a generated 3-layered CLT plate. In subsequent sections of this chapter, the principle of creating a FE model for CLT plates using *Abaqus* and the course of the data generating process are explained. The geometry and material parameter generating sections, as parts of a *Matlab*-script file, as well as data storing variables are discussed; for exemplification code sections are listed of cited. Results of the FE calculation for a sample plate are discussed in Chapter 4 . Furthermore some example plots are presented to show the abilities of the simulation program. The thesis is closed with some conclusion and perspective for future work.

1.4 General description of CLT

Cross Laminated Timber is a massive wood product, which is made up of ordinary flat boards glued together in a cross-layered fashion (Fig. 1.1) . It is used in the field of load carrying constructions.

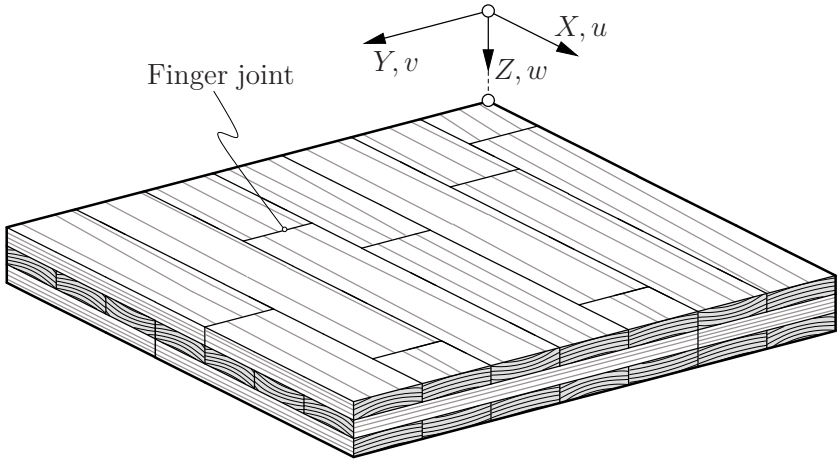

Figure 1.1: Cross laminated timber

CLT is built up by at least three layers, mostly glued together to rectangular plates, typically with a symmetric layup. Due to the characteristic assembly, the cross lying layers constrain dimensional changes of all adjacent layers result-

ing from an alternating moisture content. Therefore, high dimensional stability is reached. The boards, from which the layers are assembled, are connected by finger joints. The thickness of boards varies due to production circumstances from 12 to 45 mm. Currently, CLT is manufactured industrialy exclusively from coniferous wood. Separate layers are bonded together with polyurethane-glue. The bonding is approximately rigid.

In comparison to frame constructions the advantages of constructions built out of CLT are: smaller component heights, enabling slender but robust shear walls; enhanced sound insulation as well as improved fire protection due to the massive building material; major design flexibility based on the missing grid pattern; almost no limitations concerning the application of loads.

All the investigations in this thesis are performed for a three-layer assembly. The subsequently discussed CLT-Plates are characterized by identical layer thicknesses of both interior and surface layers.

Chapter 2

Theoretical background, input data for the computation program

Wood is a naturally grown, highly optimized material. From a microscopic view, it shows an inhomogeneous, porous structure consisting of cell wall substance and cell wall cavities. Its mechanical characteristics are pronouncedly anisotropic, which is a consequence of the elongated arrangement of the cell structure and the orientation of the cell walls. As a result of the anisotropic structure, there are widely differing mechanical properties in longitudinal and transverse direction of a log.

In this section, all calculations required for the subsequent determination of mechanical parameters as input for the simulation-program are presented. They are formulated as functions of three basic wood properties: density ρ [g/cm^3], moisture content u in [%], and influence of knots, expressed by the knot area ratio (KAR-value).

2.1 Generalized Hooke's law

For the performance of structure analysis in the framework of continuum mechanics, mechanical parameters of homogeneous wood material need to be defined. Based on the characteristics of an ideal log with its ring-wise organized cell structure (growth rings), a cylindric coordinate system is convenient for the formulation of constitutive, kinematic and kinetic relations. At the level of separate boards, the primary material directions can be defined in an orthogonal coordinate system (Fig. 2.1), because of the small board dimension and the thus negligible curvature of the growth rings.

The mechanical behavior is described in the framework of elasticity theory using Hooke's law. Assuming a hyperelasic material model, an elastic potential exists. Considering the symmetry of strains ε_{kl}, stresses σ_{ij}, and the material compliance matrix D_{ijkl} as as well as the restriction to orthogonal anisotropy, the constitutive relations are defined as

$$\varepsilon_{ij} = D_{ijkl}\,\sigma_{kl}\ , \qquad i,j,k,l = 1,2,3 \tag{2.1}$$

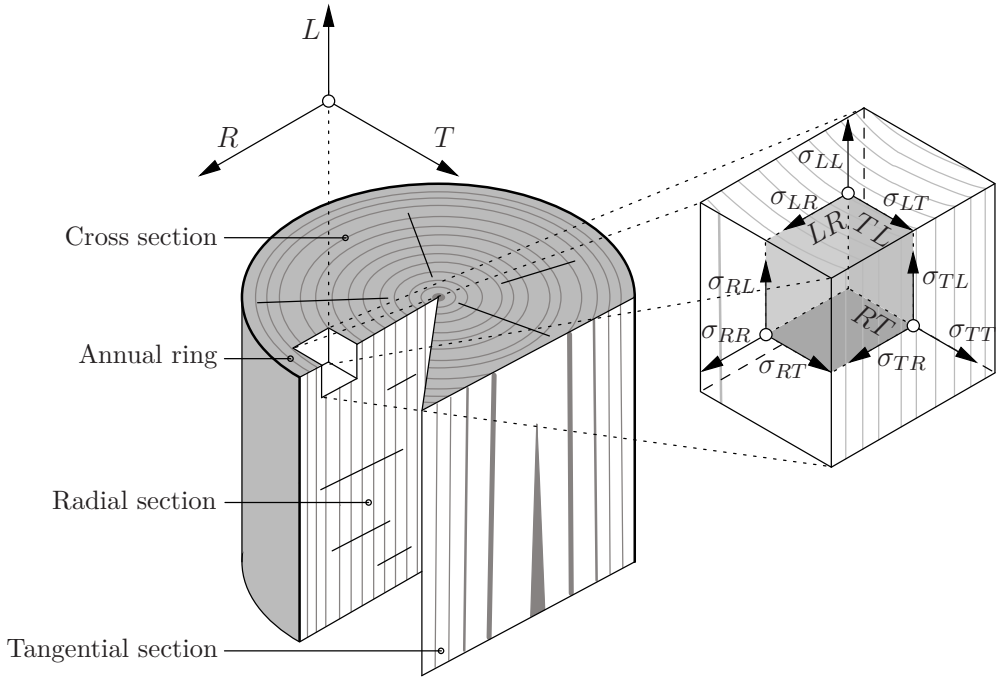

Figure 2.1: Sections of a log, primary material directions

wherein the elasticity-tensor C_{ijkl} is defined as

$$\mathbf{C} = \mathbf{D}^{-1}. \tag{2.2}$$

Expressed in matrix-notation HOOKE's law for orthotropic materials reads in a spatial formulation stress, considering the principal axes – longitudinal direction of log L (= fiber direction), radial direction R, and tangential direction T according to Fig. 2.1 – as,

$$\begin{Bmatrix} \varepsilon_L \\ \varepsilon_R \\ \varepsilon_T \\ \gamma_{LR} \\ \gamma_{RT} \\ \gamma_{TL} \end{Bmatrix} = \begin{bmatrix} \frac{1}{E_L} & -\frac{\nu_{RL}}{E_R} & -\frac{\nu_{TL}}{E_T} & 0 & 0 & 0 \\ -\frac{\nu_{LR}}{E_L} & \frac{1}{E_R} & -\frac{\nu_{TR}}{E_T} & 0 & 0 & 0 \\ -\frac{\nu_{LT}}{E_L} & -\frac{\nu_{RT}}{E_R} & \frac{1}{E_T} & 0 & 0 & 0 \\ 0 & 0 & 0 & \frac{1}{G_{LR}} & 0 & 0 \\ 0 & 0 & 0 & 0 & \frac{1}{G_{RT}} & 0 \\ 0 & 0 & 0 & 0 & 0 & \frac{1}{G_{TL}} \end{bmatrix} \begin{Bmatrix} \sigma_L \\ \sigma_R \\ \sigma_T \\ \tau_{LR} \\ \tau_{RT} \\ \tau_{TL} \end{Bmatrix}. \tag{2.3}$$

The symmetry of the material compliance matrix results in the following necessary

symmetry conditions

$$\frac{\nu_{LR}}{E_L} = \frac{\nu_{RL}}{E_R} \ , \qquad \frac{\nu_{RT}}{E_R} = \frac{\nu_{TR}}{E_T} \ , \qquad \frac{\nu_{TL}}{E_T} = \frac{\nu_{LT}}{E_L} \ . \tag{2.4}$$

Nine independent mechanical parameters are sufficient to formulate a constitutive law for orthotropic materials: module of elasticity E_L, E_R, E_T, POISSON's ratios ν_{RL}, ν_{RT}, ν_{TL}, and shear moduli G_{LR}, G_{RT}, G_{TL}.

2.2 Modulus of elasticity, shear-modulus and Poisson's ratio

Mechanical properties, like strength and stiffness values of wood, are determined from the technological parameters bulk density, moisture content, as well as influence of knots and growth imperfection. A micromechanical model was developed at the IMWS, which enables the determination of elastic mechanical parameters of clear wood (without knots or other growth irregularities) according to the aforementioned two main influencing values density ρ and moisture content u. Subsequently the nine independent elastic parameters E_L, E_R, E_T, ν_{LR}, ν_{RT}, ν_{TL}, G_{LR}, G_{RT}, G_{TL} are defined in dependency of ρ and u. The particular influence of the latter two parameters on individual elastic constants is determined from regression equations based on the micromechanical model predictions for spruce wood:

$$\begin{aligned}
E_L &= 9221\,(\ 0.0099\,\rho^2 + 2.2171\,\rho + 0.0003\,)\,(\ 0.3586\,u^2 - 1.4994\,u + 1.2853\,)\\
E_R &= 474\,(\ 8.8179\,\rho^2 - 2.4399\,\rho + 0.3067\,)\,(\ 1.4053\,u^2 - 6.0702\,u + 2.1586\,)\\
E_T &= 319\,(\ 8.7603\,\rho^2 - 2.0279\,\rho + 0.1377\,)\,(\ 1.5297\,u^2 - 6.2122\,u + 2.1822\,)\\
G_{LR} &= 587\,(\ 0.7135\,\rho^2 + 1.8226\,\rho + 0.0351\,)\,(\ 0.3576\,u^2 - 2.4174\,u + 1.4697\,)\\
G_{RT} &= 34\,(\ 21.887\,\rho^2 - 12.047\,\rho + 1.9763\,)\,(\ 1.7218\,u^2 - 6.4270\,u + 2.2176\,)\\
G_{TL} &= 576\,(\ 0.7135\,\rho^2 + 1.8226\,\rho + 0.0351\,)\,(\ 0.3576\,u^2 - 2.4174\,u + 1.4697\,)\\
\nu_{LR} &= 0.3314\,(\ -0.3026\,\rho^2 - 0.7715\,\rho + 1.4086\,)\,(\ -5.6132\,u^2 + 1.8779\,u + 0.8380\,)\\
\nu_{RT} &= 0.7305\,(\ 3.4835\,\rho^2 - 4.7469\,\rho + 2.4319\,)\,(\ 1.6248\,u^2 + 0.2281\,u + 0.8902\,)\\
\nu_{RT} &= 0.0128\,(\ -2.2411\,\rho^2 + 4.9597\,\rho - 0.7771\,)\,(\ -9.4366\,u^2 - 0.2391\,u + 1.4210\,)
\end{aligned} \tag{2.5}$$

The reduction of elastic parameters in consequence of influence of knots is discussed in Subsection 2.4 .

Table 2.1: Reference strength values

Type of strength, direction	Symbol	[N/mm^2]	ρ [g/cm^3]	Reference
Uniaxial tension, longitudinal	$f^{ref}_{yt,L}$	85.41	0.43	[Eberhardsteiner, 2002]
Uniaxial tension, radial	$f^{ref}_{yt,R}$	2.56	0.43	[Kühne, 1955]
Uniaxial tension, tangential	$f^{ref}_{yt,T}$	4.23	0.43	[Kühne, 1955]
Uniaxial compression, tangential	$f^{ref}_{yc,L}$	49.98	0.38	[Eberhardsteiner, 2002]
Uniaxial compression, radial	$f^{ref}_{yc,R}$	4.20	0.43	[Kühne, 1955]
Uniaxial compression, tangential	$f^{ref}_{yc,T}$	5.60	0.43	[Kühne, 1955]
Shear, longitudinal-radial	$f^{ref}_{y,LR}$	8.25	0.38	[Eberhardsteiner, 2002]
Shear, longitudinal-tangential	$f^{ref}_{y,LT}$	8.25	0.38	[Eberhardsteiner, 2002]
Shear, radial-tangential	$f^{ref}_{y,LR}$	2.50	0.38	approximated

2.3 Strength values

Along the lines of the elastic parameters, also the influence of density on the strength values is determined by means of the micromechanical model for spruce wood. Influence functions (Fig. 2.2), controlled by the density and generated with a constant moisture content of $u = 12\%$, are multiplied by reference strength values for clear wood (Tab. 2.1), which gives the sought strength values without influence of knots (2.6).

$$\begin{aligned}
f_{yt,L} &= f^{ref}_{yt,L}\ fs_{t,L}(\rho), \quad f_{yt,R} = f^{ref}_{yt,R}\ fs_{t,R}(\rho), \quad f_{yt,T} = f^{ref}_{yt,T}\ fs_{t,T}(\rho) \\
f_{yc,L} &= f^{ref}_{yc,L}\ fs_{c,L}(\rho), \quad f_{yc,R} = f^{ref}_{yc,R}\ fs_{c,R}(\rho), \quad f_{yc,T} = f^{ref}_{yc,T}\ fs_{c,T}(\rho) \\
f_{y,LR} &= f^{ref}_{y,LR}\ fs_{LR}(\rho), \quad f_{y,LT} = f^{ref}_{y,LT}\ fs_{LT}(\rho), \quad f_{y,RT} = f^{ref}_{y,RT}\ fs_{RT}(\rho)
\end{aligned} \tag{2.6}$$

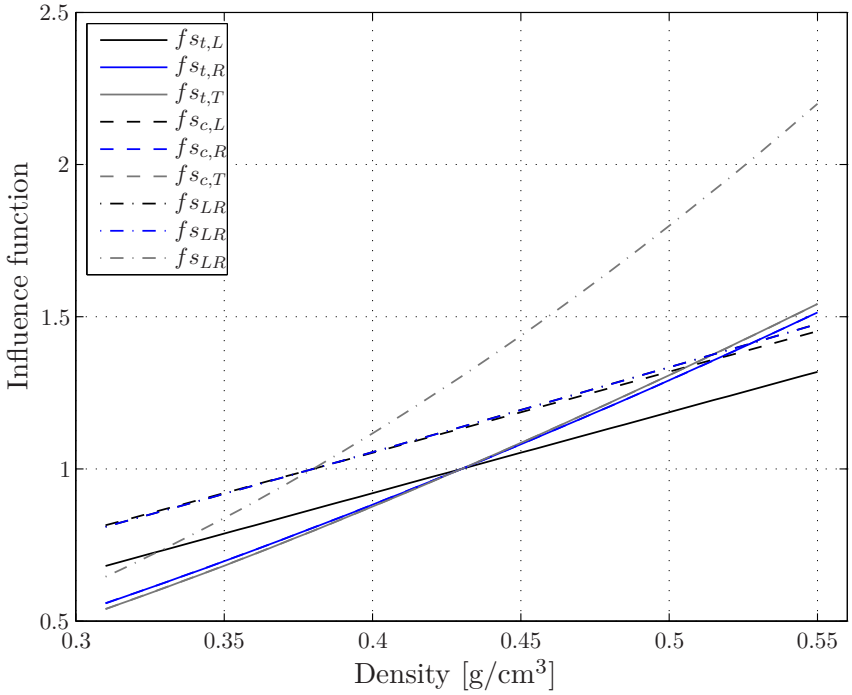

Figure 2.2: Influence functions versus density

The reduction of strength values in consequence of influences of knots is discussed in subsection 2.4 .

2.4 Influence of knots

Mechanical properties of wood are significantly reduced by the influence of knots. This influence on clear wood properties is estimated by means of the Knot Area Ratio (KAR-value). The value is defined as the sum of the cross-sectional area of knots related to the overall cross-sectional area of a board (see Fig. 2.3):

$$KAR = \frac{A_1 + A_2}{b\ h} \tag{2.7}$$

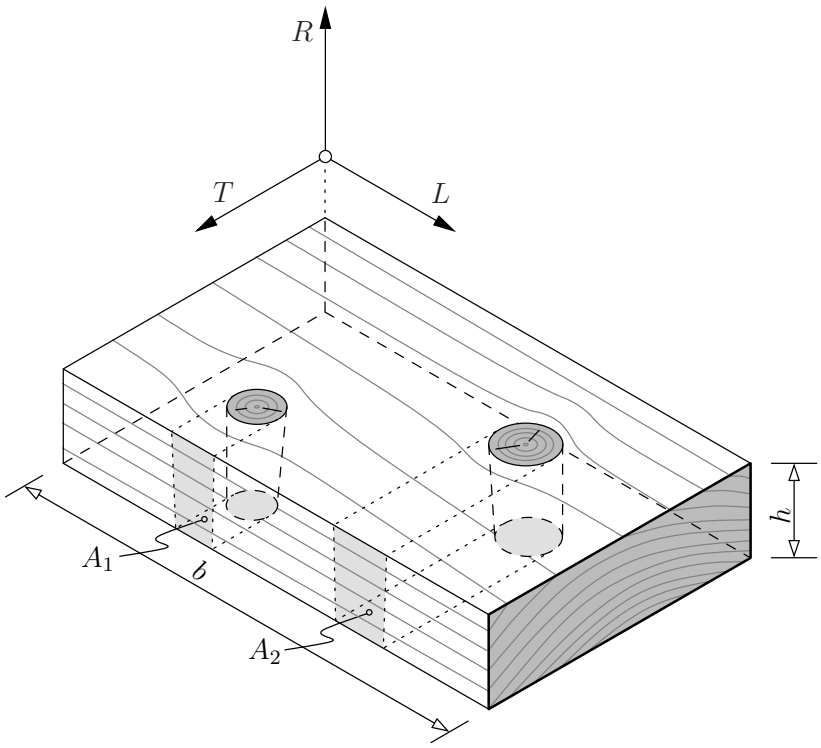

Figure 2.3: KAR

2.4.1 Reduction of modulus of elasticity and shear-modulus

To consider the influence of knots on all nine elastic constants, approximate reduction ratios are defined. Two reduction ratios are defined as apparent from Fig. 2.4 : k_l specifies the ratio between knot area and clear wood area in longitudinal direction. For the reduction of elastic constants in relation to the tangential plane (L–T - plane), k_q ist defined as ratio between diameter of knot and a circle with diameter of l. This results in

$$k_l = \frac{l-d}{l}\,, \qquad k_q = \frac{l^2 - \pi\dfrac{d^2}{4}}{l^2}\,. \tag{2.8}$$

Using the definition of the KAR-value (Fig. 2.3) the reduction ratios can be written as follows:

$$k_l = 1 - KAR\,, \qquad k_q = 1 - \pi\,\frac{KAR^2}{4}\,. \tag{2.9}$$

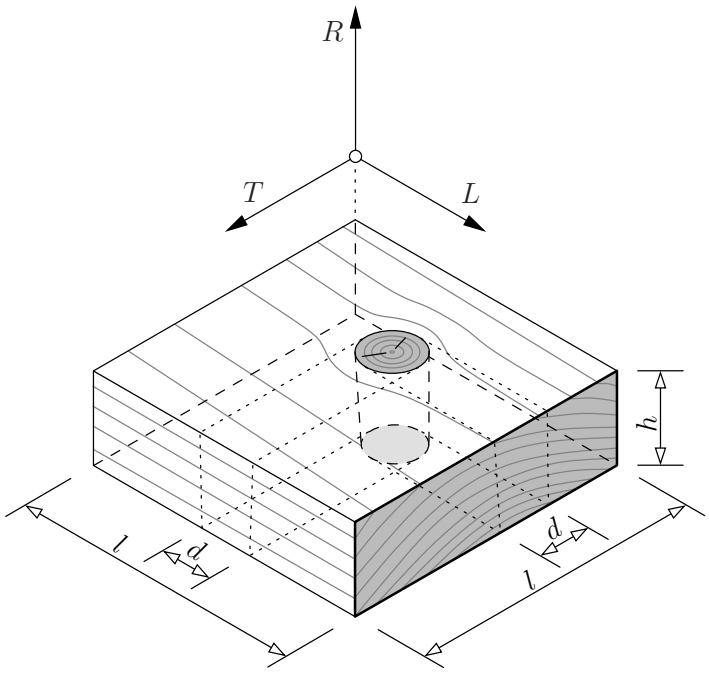

Figure 2.4: Representative knot-dimensions

The moduli of elasticity are reduced as follows:

$$\begin{aligned} E_L^k &= k_l \; E_L\,, \qquad & E_R^k &= k_q \; E_R\,, \qquad & E_T^k &= k_l \; E_T \\ G_{LR}^k &= k_l \; E_{LR}\,, \qquad & G_{LT}^k &= k_l \; E_{LT}\,, \qquad & G_{RT}^k &= k_l \; E_{RT} \end{aligned} \tag{2.10}$$

It is assumed that Poisson's ratios ν_{LR}, ν_{RT} and ν_{TL} are not affected by knots.

2.4.2 Reduction of strength values

The strength values in (2.6) hold for clear, i.e. knot-free wood. The reduction of the uniaxial tensile strengths in consequence of knots is determined as

$$\begin{aligned} f_{yt,\,L}^k &= f_{yt,\,L} \;\; e^{-2.78 \;\; KAR}\,, \\ f_{yt,\,R}^k &= f_{yt,\,R} \;\; e^{-4.56 \;\; KAR}\,, \\ f_{yt,\,T}^k &= f_{yt,\,T} \;\; e^{-4.56 \;\; KAR}\,. \end{aligned} \tag{2.11}$$

According to experimental results of [Fleischmann, 2005], describing the reduction of the uniaxial compression strength in consequence of knots, data are qualitatively specified in (2.12), wherein $rc = 50$. Experimental values are listed in Tab. 2.2 .

Table 2.2: Experimental values in [N/mm^2]

	L	R	T - direction
$f_{yc}^{k,ex}$	30.50	3.48	3.48
f_{yc}^{k}	46.20	5.15	5.15

$$
\begin{aligned}
f_{yc,L}^{k} &= \frac{f_{yc,L}^{k,ex}}{f_{yc,L}^{ex}}\, f_{yc,L} + (f_{yc,L} - \frac{f_{yc,L}^{k,ex}}{f_{yc,L}^{ex}})\, e^{-rc\ KAR} \\
f_{yc,R}^{k} &= \frac{f_{yc,R}^{k,ex}}{f_{yc,R}^{ex}}\, f_{yc,R} + (f_{yc,R} - \frac{f_{yc,R}^{k,ex}}{f_{yc,R}^{ex}})\, e^{-rc\ KAR} \quad . \\
f_{yc,T}^{k} &= \frac{f_{yc,T}^{k,ex}}{f_{yc,T}^{ex}}\, f_{yc,T} + (f_{yc,T} - \frac{f_{yc,T}^{k,ex}}{f_{yc,T}^{ex}})\, e^{-rc\ KAR}
\end{aligned}
\tag{2.12}
$$

Considerations based on MOHR's circle are exploited in order to describe the influence of knots on the shear strengths. With clear wood values $f_{y,ij}$, $f_{yt,j}$, $f_{yc,j}$ – $i,j \in \{L,R,T\}$, the angle ϕ_{ij} is defined as

$$
\phi_{ij} = tg^{-1}\, \frac{2\, f_{y,ij}}{f_{yt,j} - f_{yc,j}}\ , \tag{2.13}
$$

according to Fig. 2.5 . Rearranging of (2.13) with reduced uniaxial strength values for wood with knots and assuming constancy of the angle ϕ_{ij}, results in

$$
f_{y,ij}^{k} = \frac{f_{yt,j}^{k} - f_{yc,j}^{k}}{2}\ tg\,(\phi_{ij})\,, \tag{2.14}
$$

and specifying (2.14) for different principal material directions yields the sought shear strength values:

$$
\begin{aligned}
f_{y,LR}^{k} &= \frac{f_{yt,R}^{k} - f_{yc,R}^{k}}{2}\ tg\,(\phi_{LR}) \\
f_{y,LT}^{k} &= \frac{f_{yt,T}^{k} - f_{yc,T}^{k}}{2}\ tg\,(\phi_{LT}) \quad . \\
f_{y,RT}^{k} &= \frac{f_{yt,T}^{k} - f_{yc,T}^{k}}{2}\ tg\,(\phi_{RT})
\end{aligned}
\tag{2.15}
$$

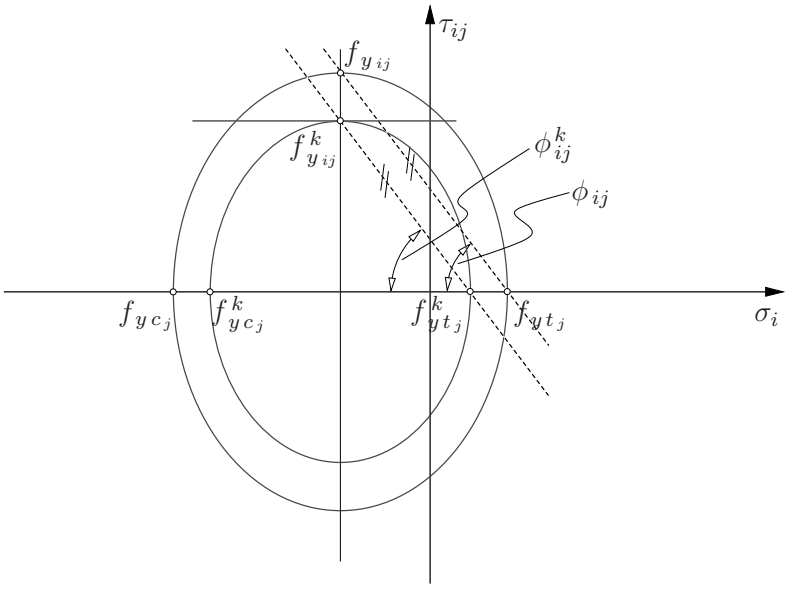

Figure 2.5: MOHR's circle for clear wood and wood with knots

2.5 Assembly of Cross Laminated Timber

As mentioned in the beginning, the investigations in this work are performed for a three-layer assembly (Fig. 1.1) . The individual layers are built up of so called «endless lamellae», where the direction of wood fibres of the surface layers correspond to the global X-axis; the direction of wood fibres of the interior layer corresponds to the global Y-axis, and the plate normal direction maps the Z-axis (Fig 2.6) .

The endless lamella is made up of «boards» with variable length, which are connected by means of finger joints on their face sides. The simulation process depicted in Chapter 3 uses a different, theoretical approach than in the industrial production process, where CLT is built up plate-wise and cutted to size in the end. In this approach, each simulated CLT is built up of «one» endless lamella. Only quadratic plates are considered. The lamella is divided into sections of length «plate width». With these sections the CLT is built up in a consecutive manner, as depicted in Fig 2.6 . The first section of the lamella starts at the origin of the global X–Y–Z - coordinate system, with its longitudinal direction aligned in X-direction. This is followed by section two, arranged in a parallel manner in the same direction, and so on. When the last section of the lamella in layer 1 is arranged, and so the dimension in Y - direction of the plate is reached, the same sequence is done to assemble layer 2, by arranging the longitudinal direction of the lamella sections in Y - direction. To specify KAR-values over the length of an

endless lamella, it is partitioned in cells (in this thesis so-called «bricks»), which have a fixed length of 150 mm (Fig. 2.6) . Though, the length of the boards the lamella is built of, are randomly generated in order to mimic the available boards in a factory for producing CLT as furhter laid down in Subsection 2.5.1 . Since brick units are used for assignment of technological parameters (density ρ, KAR-value, moisture content u) in the simulation described in Chapter 3, the randomly calculated board length within the endless lamella has to be rasterized (detail in Fig 2.6), i. e. subdivided into bricks.

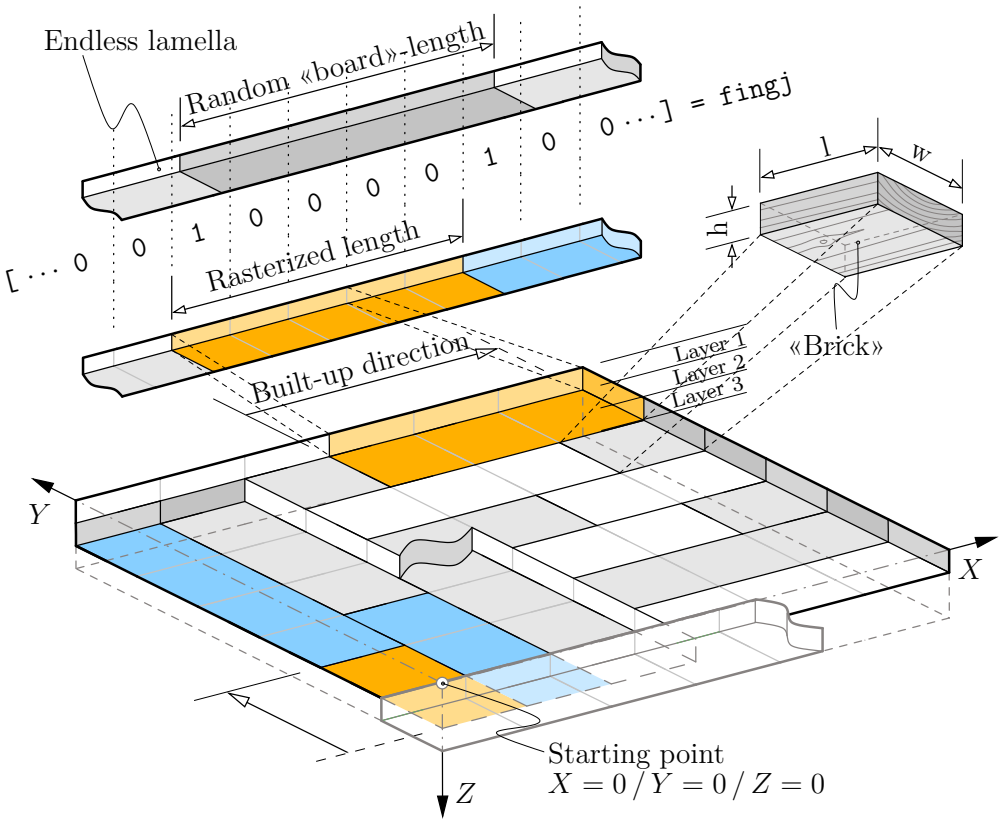

Figure 2.6: Assembly, bottom view

The boards, the lamella is built up, have widths of 150 mm and thicknesses of 35 mm . Hence, the dimension of a brick are defined in line with Figs. 2.4 and 2.6 , as

$$150\,\text{mm} \quad / \quad 150\,\text{mm} \quad / \quad 35\,\text{mm} \; .$$

[l – length, L-direction / w – width, R-direction / h – height, T-direction]

CLT is built up of boards with varying technological parameters. For the numerical simulation of the plate moisture content u and bulk density ρ are specified for each particular board of an endless lamella, while – as mentioned before – the KAR-value is assigned to each brick.

Based on these parameters, mechanical parameters of each board are calculated (Sec. 2.2 – 2.4) . For the moisture content, a constant value according to standard ambient condition and air humidity of $u = 12\,\%$ is chosen for all boards within the endless lamella. The mechanical characteristic of wood under tensile load is approximately linear elastic, until a brittle fracture occurs (Fig. 2.7, graph (a)) . Hence, to represent the mechanical failure behavior of CLT, cohesive elements are integrated in sections, where tension stress occurs. For the mechanical characteristic under compression load, an ideal elastic-plastic failure model is assumed. The Tsai-Wu failure criterion [Radecki-Pawlik, 2009] suitably describes the onset of failure in orthotropic materials. Since plastic failure in compression never occured in the simulations discussed in the following chapters, the theoretical background of plastic failure is not presented in further detail in this thesis.

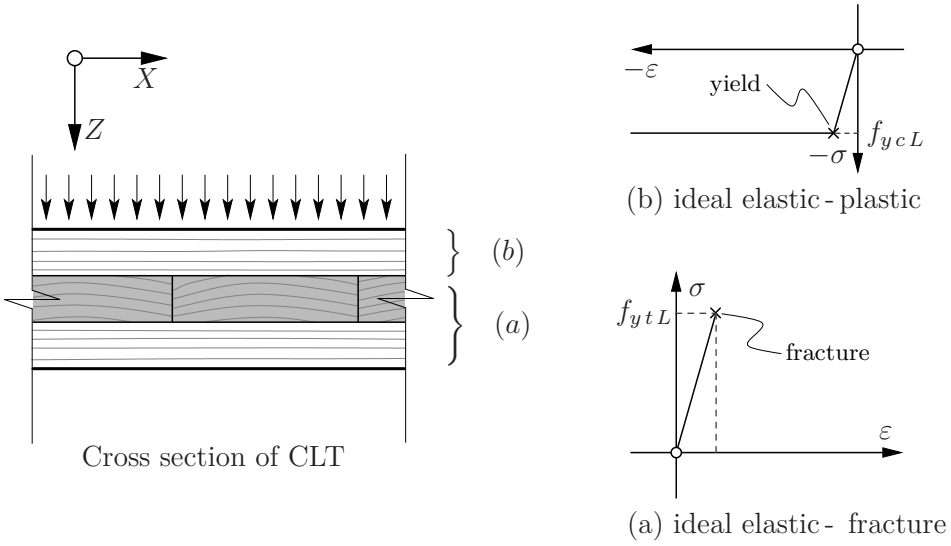

Figure 2.7: Material model

2.5.1 Position of finger joints – lengths of boards

To calculate the length of each specific board, the same statistical distribution as in [Ehlbeck et al., 1985] is employed. The latter distribution is determined by an evaluation of board lengths used in Danish glulam beams manufacturing companies.

The board lengths are normal distributed with average $\mu = 4.30\,\mathrm{m}$ and standard deviation $\sigma = 0.71\,\mathrm{m}$. Boards longer than $6.30\,\mathrm{m}$ and shorter than $2.40\,\mathrm{m}$ are disregarded in the simulation of the endless lamellae. So, for the simulation of the endless lamellae, boards with above described distributed lengths are randomly chosen and bonded together.

2.5.2 Density of boards

Analogous to the specific board lengths within the endless lamellae, also the density ρ of each board is chosen randomly. It is assumed that each board in the endless lamella has a constant density over the whole board length. This simplification is based upon experiments [Ehlbeck et al., 1985], in which it was demonstrated that, within 80 % of a control sample of 111 boards, the variation of the density between respective board endings is lower than 4 %. According to the same experiments [Ehlbeck et al., 1985], the average density of spruce wood was determined to be normal distributed with $\mu = 0.43\,\mathrm{g/cm^3}$ and $\sigma = 0.05\,\mathrm{g/cm^3}$.

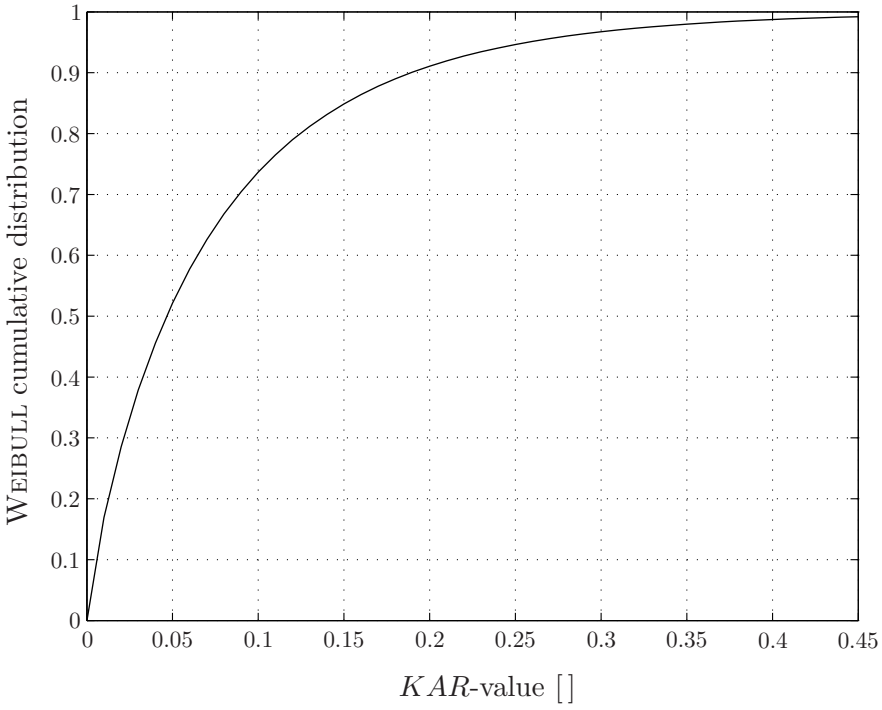

Figure 2.8: Weibull cumulative distribution of KAR-values

2.5.3 *KAR*-values of bricks

Contrary to the constant density ρ over the entire board, the KAR-value varies within the board and is assigned at brick level. The frequency distribution of the KAR-values is defined based on an evaluation of 468 samples (see [Ehlbeck et al., 1985]), related to the visual grade class II of wood. The values range from 0 up to 0.45, and they are approximately WEIBULL distributed, wherein

$$f(x\,|\,a,b) = b\,a^{-b}\,x^{b-1}\,e^{-(\frac{x}{a})^b}\,I_{(0,\infty)}(x) \tag{2.16}$$

is the WEIBULL probability density function (see [Matlab Documentation, 2009]) , with scale parameter $a = 0.0714$ and shape parameter $b = 0.8565$. The corresponding cumulative distribution of Eq. (2.16) is presented in Fig. 2.8 . Hence, each brick has a randomly chosen KAR-value out of the range $0 < KAR < 0.45$.

Chapter 3

Simulation-program

In this section, both the aim and the functionality of the simulation program are outlined. The FE-model is established in order to compute deflections, stresses, and strains of CLT plates. To simulate the CLT plates, FE software *Abaqus* ^{TM} is used in version 6.9-2 .

The simulation program is used to build up the FE-model of quadratic, three-layer CLT plates with characteristic technological and design properties as laid down in Section 2.5 . By means of mesh density parameters for all sections of the assembly, the fineness of the mesh and, thus, the number of elements used to discretize one brick, can be specified. Mechanical parameters (such as elastic material parameters and strength values) are calculated for each brick (Fig. 2.6), serving as lowest unit for assignment of technological parameters (such as density ρ).

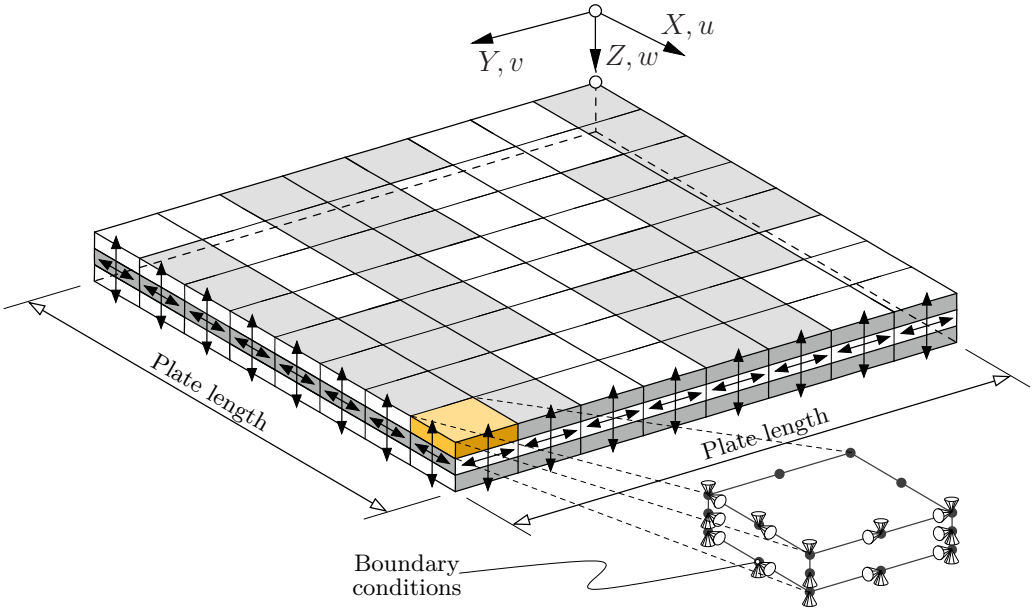

Figure 3.1: Boundary conditions

In Fig. 3.1 the FE-model of a plate, generated with the simulation program and constrained with boundary conditions, is presented. The default boundary conditions used in this thesis and depicted in Fig. 3.1 allow displacements of the nodes only perpendicular to the edges in the plate plane. The directions of arrows displayed at lateral faces of the plate represent the restricted degrees of freedom. In mechanical terms, this means:

$$\text{at surface} \quad x = 0 \;\text{ and }\; x = \langle \textit{plate width} \rangle : \; u = 0 \,,$$

$$\text{at surface} \quad y = 0 \;\text{ and }\; y = \langle \textit{plate width} \rangle : \; v = 0 \,.$$

A distributed load is standardly applied to the topside of the plate (Fig. 3.2).

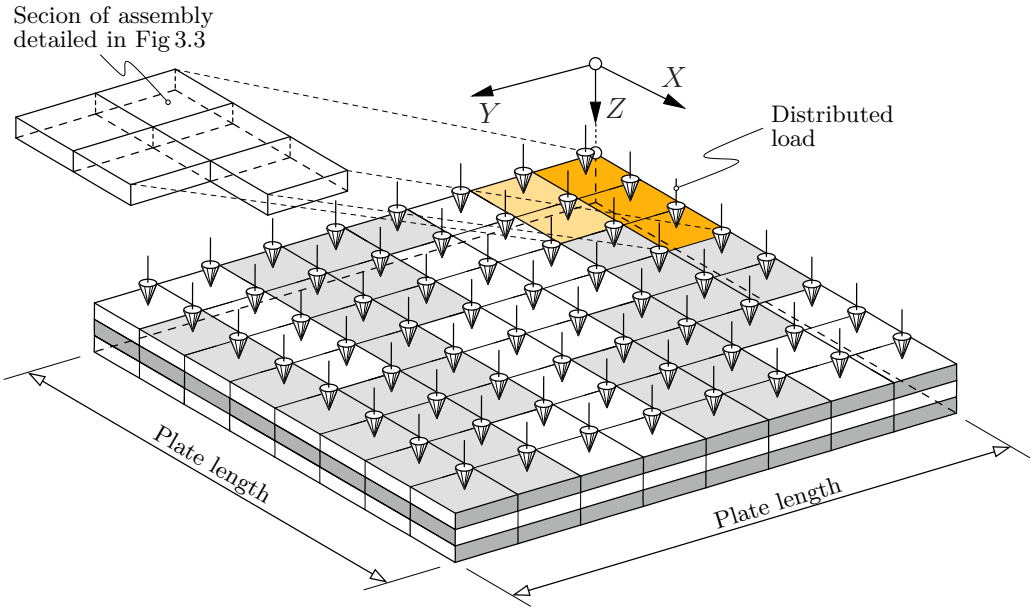

Figure 3.2: Distributed load

The theoretical background of the material behavior used in the framework of the FE calculations is discussed in Chapter 2. To implement the mechanical failure model of CLT under uniformly distributed load, cohesive elements are integrated in layer 2 and layer 3 (Fig. 2.6), where tension stresses occur. According to Section 2.5 , mechanical parameters are randomly assigned to the bricks, wherein the elastic parameters, according to the linear theory of elasticity (Section 2.1), are calculated from the technological parameters density ρ, KAR-value, and moisture content u (Sec. 2.5). Strength values assigned to the cohesive elements, are calculated according to Section 2.3 . The strength values are required for evaluating the nominal

stress criterion of damage initiation of cohesive elements. They are calculated analogous to the elastic parameters, from the technological parameters (ρ, KAR, u) of adjacent bricks, whereas the values are taken from the weakest respective adjacent brick .

3.1 Principle of modeling

In the FE model, two types of elements are used: Three-dimensional solid stress/displacement elements, for describing elastic material behavior, and cohesive elements, which enable to create cracks in surface layers when a critical tension stress is exceeded. Figure 3.3 shows a section of the exterior layer 1 (Fig. 3.2) of the schematic assembly of CLT used for the FE-simulation. Note, that in Fig. 3.3 as well as in all subsequent figures the angle of view is changed: In all figures depicting mesh generating details, the Z-axis is directed bottom-up.

All «bricks» as specified in Sec. 2.5 are encased by cohesive elements. The blue, green, and orange planes in Fig. 3.3 are representing geometrical sections of cohesive elements. Even though cohesive elements are composed of two faces (see Fig. 3.7), they are displayed planar in Fig. 3.3 in a schematical manner. For a better illustration of sections in Fig. 3.3, the orange cohesive section is only depicted once. It is required, that the rectangularly assembled solid bricks are encased by these cohesive elements in order to be able to reproduce the cracking process. Otherwise, if cohesive elements are only located between bricks in longitudinal direction of the endless lamella (green cohesive sections in Fig. 3.3), the crack process doesn't start due to constraints at the corner nodes of the solid section bricks.

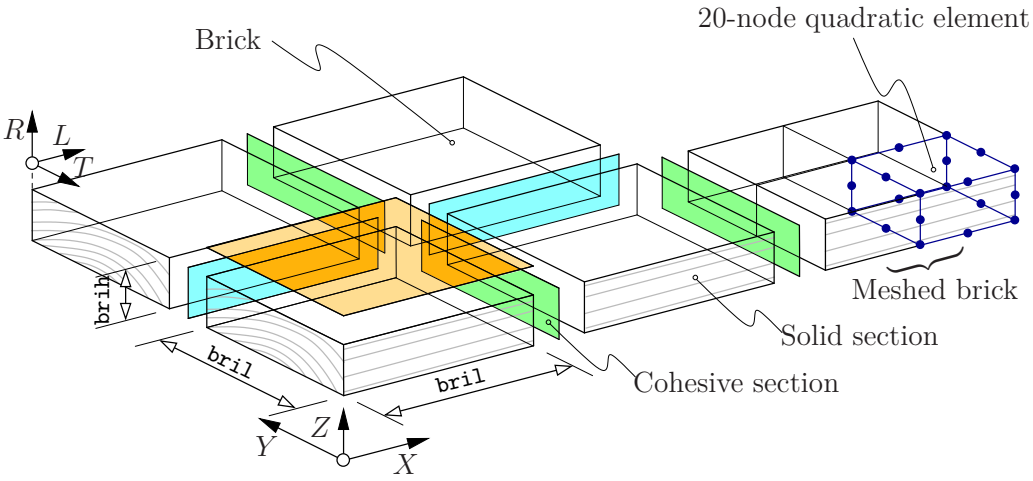

Figure 3.3: Assembly of cohesive and solid sections

So, the FE model is built up of rectangularly arranged copies (from now on named assembly) of the following four geometrical sections as shown in Fig. 3.3: the solid section brick with cuboid shape, which is meshed with three-dimensional solid stress/displacement elements; the cohesive interface between solid bricks in X–Z - plane (blue); the cohesive interface in longitudinal direction in Y–Z - plane (green); the cohesive interface between layers in X–Y - plane (orange). In the simulation program, parameters are assigned to these sections, where all finite elements inside the section have identical material parameters. As already mentioned, the mesh density is variable in the solid section as well as in the cohesive section. For example, in Fig. 3.3 a solid section brick meshed with density of «four elements per brick» is shown; the nodes of a *C3D20*-solid stress/displacement element are plotted. To build up the assembly of these sections, a global coordinate system is introduced. The relation between the local L–R–T - system, for bricks in layer 1, and the global X–Y–Z - system is also apparent in Fig. 3.3 .

To apply boundary conditions and loads to the FE-model of CLT, miscellaneous sets of nodes and elements are defined within the simulation program. Two examples: one node set is generated for each of the lateral edges; to apply distributed load (Fig. 3.2) to the top side of the plate, an element set of the top layer is compiled. These node sets are defined after the mesh has been built. The amplitude of loads, the degrees of freedoms for which boundary conditions apply, as well as other parameters such as control values for solution techniques, are set in the the last subsection of the program, the so called «history definition» pursuant to *Abaqus* notation. In the input section of the simulation program, parameters defining dimensions are specified in [mm], and parameters defining loads are specified in $[\mathrm{N/mm^2}]$.

For the FE analysis by *Abaqus/Standard* ^{TM}, there are two options how to handle the input process. The first option is to design the model section with the integrated computer aided engineering (CAE) application. This is advantageous in most cases because it is easy to define all aspects of the model with integrated design modules (for example, defining the geometry, defining material properties, and generating the mesh). In this way, a model is built up from which *Abaqus/CAE* generates an input-file (*job_name*`.inp`) to be submitted to the solver *Abaqus/Standard*. The second option is to generate the input-file manually (e. g. with a text editor) or in the framework of an I/O-program. The input-file contains all definitions required to perform the analysis. Representing the model in the form of keywords, the file is written in ASCII format. In this thesis, the latter option to generate the input-file is used, employing *Matlab* programming language. The big advantage of using *Matlab* ^{TM} as I/O-program is the ability to conveniently allocate varying material parameters to each finite element. The disadvantage of an in principal complicated mesh generation does not take effect here considering the rectangular geometry of CLT as well as using bricks as finite elements and not prisms.

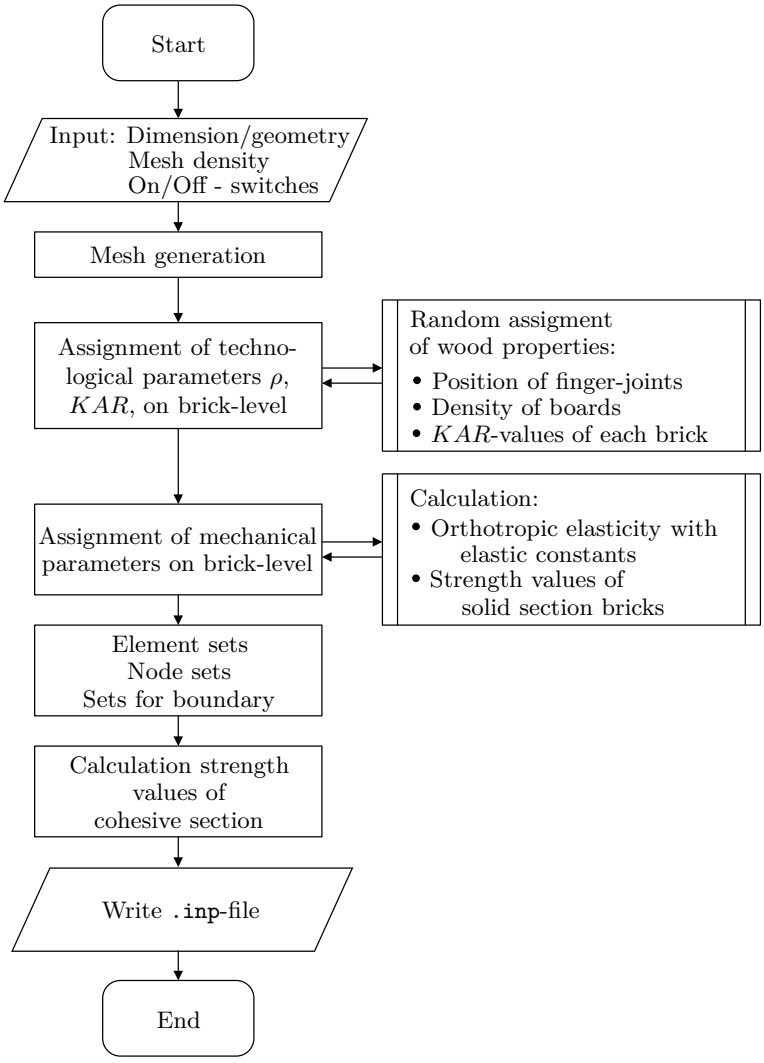

Figure 3.4: Flowchart of the *Matlab* - simulation program

The main file in *Matlab*, controlling the generation of the input file for *Abaqus*, is `inpgen.m`. The file `inpgen.m` is subdivided in several logical sections apparent in the flowchart Fig. 3.4 . In the following subsections, the detailed programming structure and the data handling are explained. All variables are commented at the beginning of the `inpgen.m`-script file; variables only used in subroutines are commented in the corresponding function file.

Matlab is optimized for matrix manipulations. Therefore all data are stored as compact as possible in form of arrays to reduce the quantity of variables.

3.2 Mesh generating section

At the beginning of the `inpgen.m`-script-file, all required geometry data are specified. The parameters `bril` = 150, `brih` = 35 define the dimensions of a brick according to Fig. 3.3; units are set in [mm]. The parameter `bripsi` defines the number of rectangularly arranged bricks per side in X and Y- direction. An equal number of bricks is assumed in the two directions, so that only quadratic plates can be simulated. Accordingly `brilay` defines the number of layers generated. In this simulation only `brilay` = 3 is supported for a correct functionality. The parameters `epbrxy`, `epbrz` determine the mesh density of the solid brick (e. g. the meshed brick in Fig. 3.3 with four *C3D20*-elements per brick is generated with `epbrxy` = 2, `epbrz` = 1).

Listing 3.1: Mesh generating section 1

```
dcon=[bril/epbrxy*0.5, brih/epbrz*0.5]

for briz=1:brilay
  for brixx=1:bripsi
    for briyy=1:bripsi

brinr=sprintf('%d%02d%02d%d',1,brixx,briyy,briz)
brinr=str2double(brinr)

stbr(1)=(brixx-1)*(bril+brimxy)
stbr(2)=(briyy-1)*(bril+brimxy)
stbr(3)=(briz-1)*(brih+brimz)

for knodez=3:2:(epbrz*2+1)
  for inodex=3:2:(epbrxy*2+1)
    for jnodey=3:2:(epbrxy*2+1)

stbr(1)=(brixx-1)*(bril+brimxy)
stbr(2)=(briyy-1)*(bril+brimxy)
stbr(3)=(briz-1)*(brih+brimz)

elenr=sprintf('%d%d%d',(inodex-1)/2,...
  (jnodey-1)/2,(knodez-1)/2)
elenr=str2double(sprintf('%05g%s',brinr,elenr))
```

In a similar way, the mesh density of the cohesive interfaces (three types; shown as blue, green, and orange layers in the figure) is controlled by `covpxy`, `covpz`,

`cohpxh`. With `brimxy`, the thickness of the cohesive layer aligned in, X–Z, Y–Z - direction is specified (blue and green planes in Fig. 3.3). Similar the thickness of the cohesive layer aligned in X–Y - direction (orange), is specified with `brimz`. `dcon(1)` stands for the half length of a solid element in X and Y - direction, `dcon(2)` for the half length in Z - direction, respectively.

The generation of nodes with specification of their coordinates is organized on two levels (List. 3.1). First, three `for`-loops on the «brick level» control the number of the bricks in each of the three orthogonal directions X, Y, and Z. Therein the range of the loops is controlled by the number of rectangularly arranged bricks per side, specified by the parameters `brilay` in Z - direction, and `bripsi` in X and Y - direction, respectively.

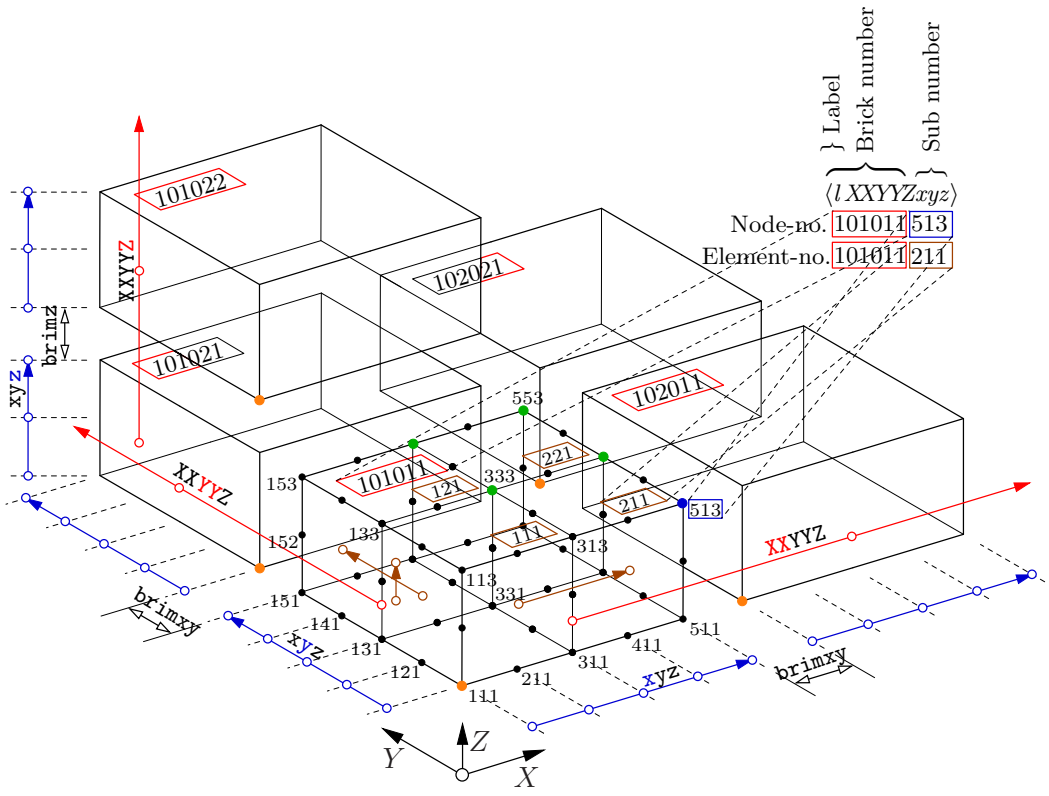

Figure 3.5: Syntax of element- and node-numbering

The current number of the brick is stored in the control variables `briz`, `brixx`, `briyy`. These control variables build a 6-digit brick number with syntax $\langle l\,XXYYZ\rangle$, where the first digit $\langle l\rangle$ is a node label, $\langle XX\rangle$ is the placeholder for `brixx`, $\langle YY\rangle$ for `briyy`, and $\langle Z\rangle$ for `briz`. The label $\langle l\rangle = 1$ in digit 1 of the brick number rep-

resents the solid section brick. The brick with brick number `1 01022` in Fig. 3.5, therefore is placed in row 1 in X-direction ($\langle XX\rangle = 01$), in row 2 in Y-direction ($\langle YY\rangle = 02$), and in row 2 in Z-direction (thus layer 2, $\langle Z\rangle = 2$). The (global) node number is created by adding three digits (denoted as sub number in Fig. 3.5) describing the node location to the brick number. As an example, the blue marked node in Fig. 3.5 located at `513` is considered. It is associated with the first solid section brick in X-direction; hence, $\langle XX\rangle = 01$ is stored in digits 2 and 3 of the node number `1 01011 513`.

Following their digit-based syntax, brick and node numbers are stored as variables of type *character array*. To generate the brick number, the **`sprintf`**-command is used for this reason. **`str2double`** converts numbers stored as string into a numeric type number.

In each loop cycle on brick level, the coordinate of the node with number ⟨*current brick number*⟩`111` is calculated and stored in `strbr`. These first nodes in each brick are marked orange in Fig. 3.5 and serve as reference points for the subsequent calculations on the «element level». On this second level, the node coordinates of elements related to the current brick (controlled by above «brick level») and the element numbers related to the current brick are calculated and stored. The number of **`for`**-loops on the «element level» is controlled by `epbrxy` and `epbrz`, according to the number of elements in X and Y-direction and in Z-direction, respectively. The current number of the element is stored in the control variables `knodez`, `jnodey`, `inodex`.

Listing 3.2: Mesh generating section 2

```
absno = [stbr(1)+2*dcon(1)*(inodex-1)/2,...
         stbr(2)+2*dcon(1)*(jnodey-1)/2,...
         stbr(3)+2*dcon(2)*(knodez-1)/2]

nodel(01,:)=[absno(1)-2*dcon(1),...

elnonr=[111 311 331 131 113 313 333 133 ...

elnonr=elnonr+(inodex-3)*100+...
  (jnodey-3)*10+(knodez-3)*1

nodenr=nobrif(brinr,elnonr,20)
```

Element numbers are built of the current brick number, using the aforementioned syntax ⟨*l XXYYZ*⟩, and of a sub number with syntax ⟨*xyz*⟩. To generate these last

three digits $\langle xyz \rangle$, again the `sprintf`-command is used. $\langle x \rangle$, the seventh digit in the element number, refers to current control variable `inodex`. Accordingly, $\langle y \rangle$ refers to current control variable `inodey`, and $\langle z \rangle$ to `inodez`. Again the element numbering is explained by means of an example in reference to Fig. 3.5 . The brown marked element with element number `1 01011 211` is the second element in X - direction of the current brick; so $\langle x \rangle = 2$ is stored in digit 7 of the aforementioned element number `1 01011 211` .

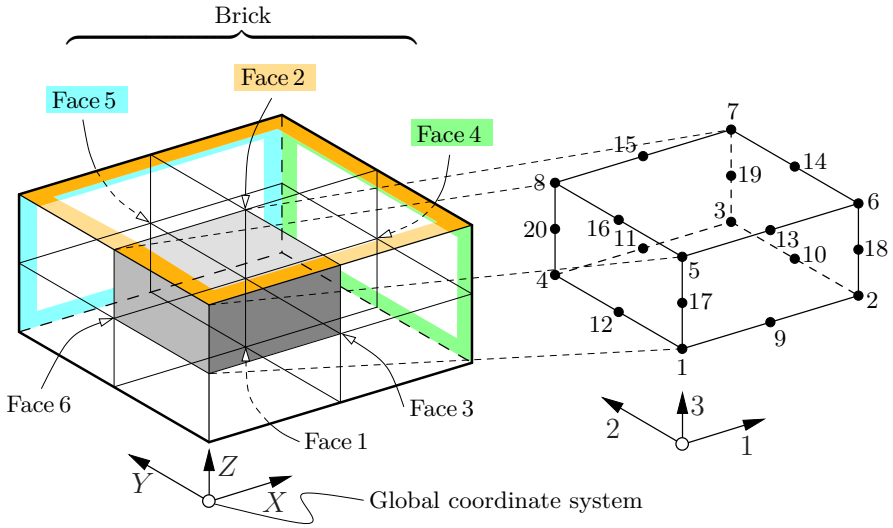

Figure 3.6: Solid section element

The calculation of the coordinates of all 20 nodes of the current element (List. 3.2) is done in the «element level» cycles (`for knodez=3:2:...`). In each loop cycle, the coordinates of reference node number 7, according to local node numbering convention are calculated and stored in `absno`. Thereby, `dcon(1)` stands for the half length of an solid element in X and Y - direction, which equals the distance between two knots. Accordingly `dcon(2)` stands for the half length of a solid element in Z - direction. The coordinates of the current element are calculated and assembled in the 20×3 - matrix `nodel`. Calculation of coordinates is done in reference to the aforementioned reference node with coordinates stored in `strbr`.

To define elements based on the nodes and to generate node sets, the local number of the nodes within an element has to be known. The local node ordering and the corresponding local coordinate system for elements in *Abaqus* is depicted in Fig. 3.6 [Abaqus Manual, 2009, 25.1.4 Node ordering and face numbering on elements]. For the interrelation between the global node number with syntax $\langle l\ XXYYZ\ xyz \rangle$ and the local node number according to the node numbering convention of solid 20-node elements, compare Fig. 3.5 and Fig. 3.6 . Reference nodes (node, with local

number 7, of Fig. 3.6) are marked green in Fig. 3.5 .

For assigning global and local node numbers, a buffer vector `elnonr` is used. This vector contains 20 sub numbers (digits 7, 8, and 9 – part $\langle xyz \rangle$ of global element number, defining the position of nodes within the element) for the 20 nodes of the current element. The sub numbers $\langle xyz \rangle$ in vector `elnonr` are sorted according to the local element node numbering of 20-node elements. Initially, they are specified for the first element (element `111` in Fig. 3.5). `elnonr` is updated, in each loop by the current control variables `knodez`, `jnodey` and `inodex`. For example, the first five sub numbers of `elnonr`, when passing through the cycle of element `1 01011 111`, are `[111,311,331,131,113,313,333,133,211,321,231, 121,213,323,233,123,112,312,332,132]`.

`nodbr1 =`

`nodnr`	`nodel`	`elenr`
⟨*brick-no.*⟩`111`	⟨*x* -, *y* -, *z* - *coordinates*⟩	⟨*element-no.*⟩
⟨*brick-no.*⟩`311`		
⟨*brick-no.*⟩`331`		
⟨*brick-no.*⟩`131`		
⟨*brick-no.*⟩`113`		
⟨*brick-no.*⟩`313`		
⟨*brick-no.*⟩`333`		
⟨*brick-no.*⟩`133`		
⟨*brick-no.*⟩`211`		
⟨*brick-no.*⟩`321`		
⟨*brick-no.*⟩`231`		
⟨*brick-no.*⟩`121`		
⟨*brick-no.*⟩`213`		
⟨*brick-no.*⟩`323`		
⟨*brick-no.*⟩`233`		
⟨*brick-no.*⟩`123`		
⟨*brick-no.*⟩`112`		
⟨*brick-no.*⟩`312`		
⟨*brick-no.*⟩`332`		
⟨*brick-no.*⟩`132`		
⟨*brick-no.*⟩`111`		⟨*element-no.*⟩
⟨*brick-no.*⟩`311`		
⟨*brick-no.*⟩`331`		
⋮	⋮	⋮

With subroutine `nobrif`, the node definition matrix `nodbr1` is built, which assigns the global number, coordinates, and the current element number to each node. The first column is made up by a vector `nodenr`, which contains the node numbers of type $\langle l\ XXYYZ\ xyz \rangle$, sorted in order of the local element node numbering: So, for exemplification, the eight nodes representing the vertices of brick

number `1 01011 211` in sequence of node ordering (Fig. 3.6) , stored in row 1 – 8 of column vector `nodenr`, are: `[1 01011 311;1 01011 511;1 01011 531;1 01011 331; 1 01011 313;1 01011 513;1 01011 531;1 01011 331;... ]`. The 20×3 - matrix `nodel` follows, containing the appropriate coordinates of the nodes. Finally, the last column of `nodbr1` includes the element numbers. The data in the vector `nodel` and the coordinate matrix are passed to the node definition matrix `nodbr1` in each element level cycle. Node numbers passed by row vector `nodenr` are stored in column 1; coordinates of the 20×3 - matrix `nodel` in column 2 – 4; the current element number `elenr` in column 5.

As noted in the beginning of this chapter, the FE-assembly is built up out of rectangularly arranged copies of four different geometrical sections: one solid section and three cohesive interface sections – marked as blue, green, and orange planes in Fig. 3.3 . The node generating commands for the solid section are depicted in detail in the previous paragraph. The node generation for cohesive elements allocated to the interface sections, proceeds in a similar way. Some details are different, and they are discussed in the following.

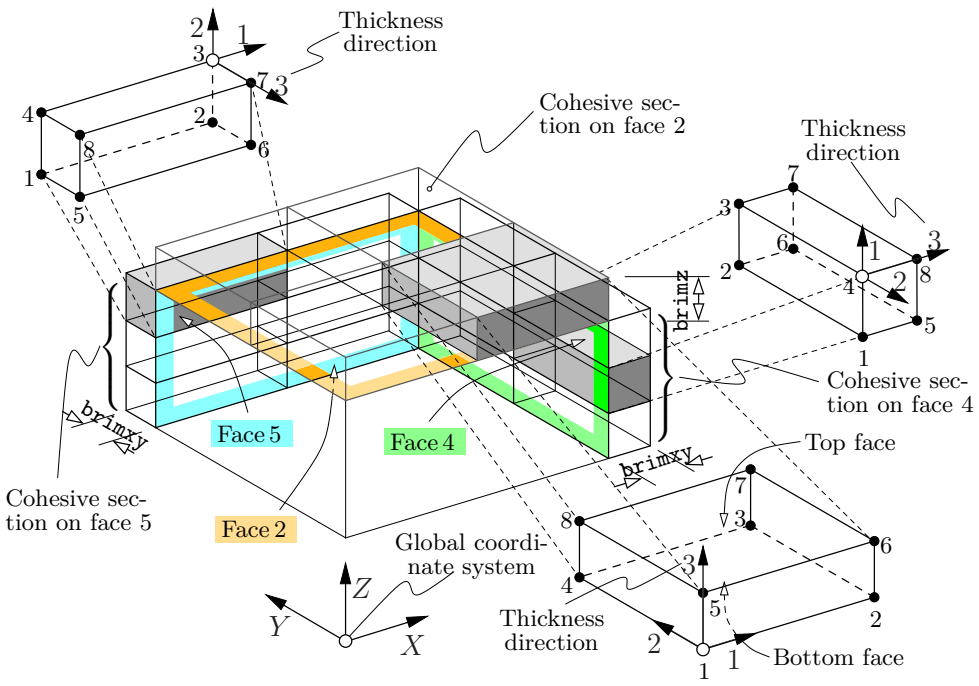

Figure 3.7: Cohesive section elements

Cohesive elements are arranged in between solid section bricks according to Fig 3.3 . For labeling of the three different cohesive interface sections, the nam-

ing convention of *Abaqus*, using local face numbers for side faces of hexahedron elements, is employed. The face labels according to Fig. 3.6 are assigned to digit 1 of the element and node numbers (Syntax $\langle l\ XXYYZ\ xyz\rangle$). For example, the identifier label in digit 1 of the element number of elements allocated to the cohesive section on face 5 is $l=$`5`; that means, that all node and element numbers allocated to the cohesive section on face 5 are of type `5`$\langle XXYYZ\ xyz\rangle$. For nodes and elements allocated to cohesive sections on face 4 and face 2, the same notation with label identifier $l=$`4` and $l=$ `2`, respectively, is used. As mentioned before, the label $l=$`1` is used for the solid sections.

Cohesive elements are composed of two faces (a bottom and a top face), separated by the cohesive zone thickness which is adjustable by the variable `brimxy` for cohesive section on face 5 and face 4, and by `brimz` for cohesive section on face 2 (Fig. 3.7) . 3D cohesive elements have nodes on their bottom face and corresponding nodes on their top face. Again, the building of elements from nodes and the generation of node sets for cohesive elements requires knowledge of the local node numbers in the element. The sequence of node ordering defines the orientation of the thickness direction (orientation of 3 - axes in Fig. 3.7) . The thickness direction of cohesive elements is always identical with the normal direction of one of the side faces 5, 4, or 2, respectively

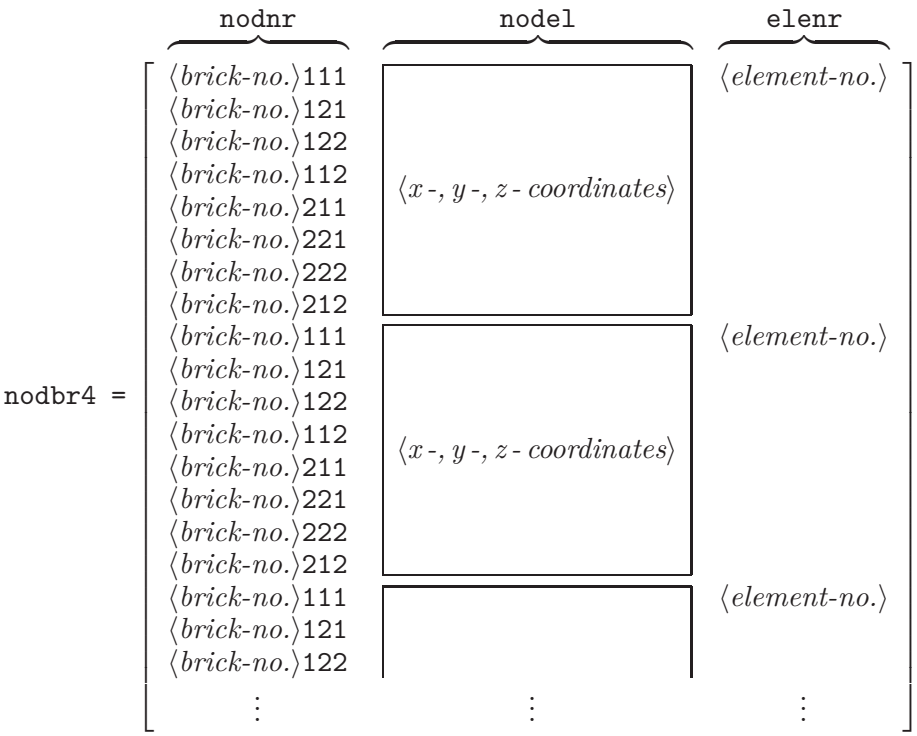

Elements within the cohesive section do not use shared nodes with solid section elements due to different mesh densities in these sections. For the order of node numbering of cohesive elements according to *Abaqus*, see Fig. 3.7. Node sets of the cohesive elements are stored in `nodbr5`, `nodbr4`, `nodbr2`, for which the format is identical to `nodbr1`. For example, nodes and elements in cohesive section on face 4 with identifier label $l = 4$ are stored in the matrix `nodbr4`.

Listing 3.3: Plot section

```
if swplot||0

  nx=nodbr1(:,2)
  ny=nodbr1(:,3)
  nz=nodbr1(:,4)

  nfx=nodel([1:4 1 5:8 5 6 2 3 7 8 4],1)
  nfy=nodel([1:4 1 5:8 5 6 2 3 7 8 4],2)
  nfz=nodel([1:4 1 5:8 5 6 2 3 7 8 4],3)

  plot3(nfx,nfy,nfz,'--k')
```

For monitoring the aforementioned mesh generating commands in a direct manner, a plot routine is integrated in the mesh generating section: The plotting function (List. 3.3) is switched on and off with the switch `swplot`. The plotting commands create a lattice model of the assembled elements. In an example plot (Fig. 3.8), nodes of cohesive elements allocated to face 5 are marked blue, nodes of cohesive section on face 4 are marked green, and nodes of cohesive section on face 2 are marked red. Edges of cohesive elements are plotted as continuous line, edges of solid elements as dashed lines.

At the end of the node generating section (List. 3.4), double node definitions in `nodbr1`, `5`, `4`, `2` are eliminated by a subroutine called `nodbrsort`. The new coordinate matrices are named `cnodbr1`, `5`, `4`, `2`:

Listing 3.4: Mesh generating section 3

```
cnodbr1=nodbrsort(nodbr1)
cnodbr5=nodbrsort(nodbr5)
cnodbr4=nodbrsort(nodbr4)
cnodbr2=nodbrsort(nodbr2)
```

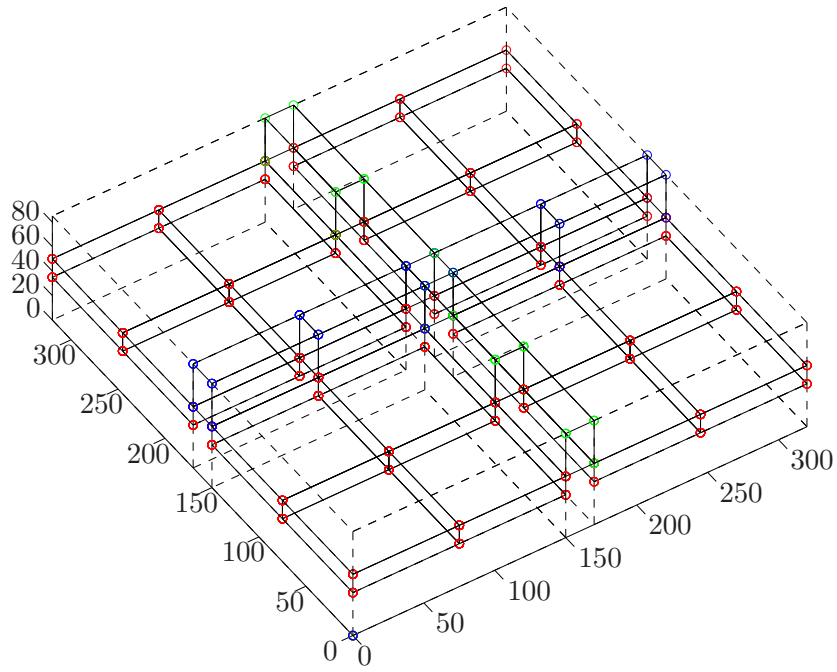

Figure 3.8: Output of plot subroutine in *Matlab*

3.3 Material and mechanical - parameter section

In this section, the procedure of calculating material and mechanical parameters is explained. A short description of relevant subroutines is given below. Material parameters are calculated from technological parameters for each brick, as the lowest unit for assignment of technological parameters (Fig. 2.6) . The parameters are calculated according to Section 2.2 for elastic parameters, and to Section 2.3 for strength values.

Listing 3.5: Material paramter section

```
laml=inlmem(5)*bril

kar=kardist(laml,bril,seed(3))

[rho,fingj]=dendist(laml,...
  bril,seed(1:2))

rho=genpar3d(rho,bripsi,brilay)
kar=genpar3d(kar,bripsi,brilay)
```

To determine and store the technological parameters (List. 3.5), density ρ, KAR-values, and the positions of finger joints for each brick, three row vectors (`rho`, `kar`, `fingj`) with dimension ⟨*bricks/plate*⟩ or equivalently ⟨*lamella-length/brick-length*⟩ are initialized – all components of these vectors are set to `0`. The length of the endless lamella is calculated in `laml`, whereat `inlmen(5)` is the counter for loop cycles on brick level. For example, the endless lamella of the CLT plate in Fig. 3.1 with 8 bricks per side (`bripsi` = 8), has an overall length of 192·⟨brick length⟩ (8·8·3 = 192 , resulting from ⟨number of bricks in the fitted lamella section⟩·⟨number of lamella sections arranged side by side⟩ · ⟨number of plate layers⟩). Thus, 192 would be stored in `inlmen(5)`. Each component of the row vectors (`rho`, `kar`, `fingj`) is allocated to a corresponding brick of the endless lamella in a consecutive manner. For understanding the relation between the endless lamellae and the built-up of CLT in this simulation, see Fig. 2.6 . In this figure, bricks, as sections of the endless lamella, and for demonstration their corresponding components in the row vector fingj are depicted.

With subroutine **`kardist`**, a KAR-value is calculated for each brick, according to the distribution discussed in Subsection 2.5.3 . To determine the positions of finger joints, the subroutine **`geodist`** calculates the randomly distributed lengths of boards, of which the endless lamella is built. The distribution of the board lengths, parameters mean value μ and standard deviation σ are set inside the subroutine function files (`geodist.m`). The distribution of board lengths is discussed in Subsection 2.5.1 . Since bricks form the lowest unit used for assignment of technological parameters, the calculated board lengths have to be rasterized into sections of the brick length as described in Section 2.5 . Bricks at board ends hold a `1` in the corresponding component of `fingj`, bricks inside the board hold a `0`. Subroutine **`dendist`** calculates the density of each brick according to Subsection 2.5.2 on basis of positions of finger joints (`fingj`) . The same also applies for the fixing of distribution parameters for board densities ρ, in `dendist.m`.

To generate random values according to a given distribution, like it is needed for the generation of the aforementioned technological parameters KAR, ρ and ⟨*length of board*⟩, random numbers are used. Pseudo random numbers in *Matlab* come from a random number stream. To reiterate plates with identical material parameters at varying mesh densities, a control value of the random number stream is set. With the parameter `simn`, defined in the input section, the control value for the random stream is determined. The triple of control values needed for the three ⟨. . . ⟩`dist.m`-subroutines are stored in the file `seed.dat` in form of a row data matrix.

`genpar3d` assembles the row vectors `kar`, `rho` and `fingj` into a multidimensional cell array with dimension '⟨*bricks/side*⟩- by ⟨*bricks/side*⟩- by ⟨*number of layers*⟩-array'. A cell array is a collection of containers called «cells» in which different types of variables can be stored. The assembly proceeds in an equivalent manner as the crosswise building of CLT out of the endless lamellae (Fig. 2.6) . For exemplification,

the illustration in Fig. 3.9 uses the concept of a page to represent a three-dimensional cell array. The size of the array ⟨4, 4, 3⟩ – ⟨*rows, columns, pages*⟩, used for the array in the figure coincide with a CLT plate with geometry `bripsi`=4 and `brilay`=3.

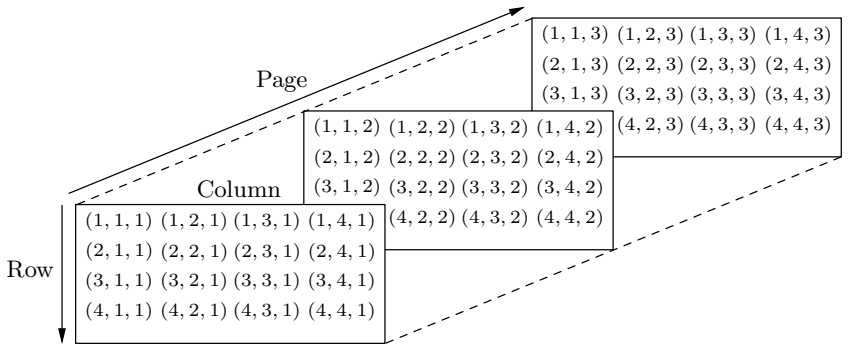

Figure 3.9: Multidimensional array in *Matlab*

The mechanical parameters such as elastic constants and strength values, calculated from technological parameters ρ and KAR with the code in List. 3.6, are stored similarly to these parameters in three-dimensional cell arrays. So, mechanical parameters of each brick are stored in a 9×12 - matrix, which is itself nested in a ⟨*bricks/side*⟩×⟨*bricks/side*⟩×⟨*number of layers*⟩ - matrix of type multidimensional cell array.

Listing 3.6: Mechanical parameter section 1

```
par=cell(bripsi,bripsi,brilay)

for briz=1:brilay
  for briyy=1:bripsi
    for brixx=1:bripsi

parwm=zeros(9,12)
parwm(7,1:9)=strength(rho(brixx,briyy,briz),...
  kar(brixx,briyy,briz))
parwm(9,1:9)=elastpar(rho(brixx,briyy,briz),...
  kar(brixx,briyy,briz))

par(brixx,briyy,briz)={parwm};  end;end;end
```

Again, loops on brick level are used to compute the mechanical parameters of each brick. Mechanical parameters are calculated by subroutines `strength` and `elastpar`. Subroutine `[stren]=strength(rho,kar)` calculates nine strength values according to Sec. 2.3 :

$$f_{yt,L}\ ,\ f_{yt,R}\ ,\ f_{yt,T}\ ,\ f_{yc,L}\ ,\ f_{yc,R}\ ,\ f_{yc,T}\ ,\ f_{yLR}\ ,\ f_{yLT}\ ,\ f_{yRT}$$

Subroutine `[p]=elastpar(rho,kar)` calculates the nine elastic constants of the current brick according to Sec. 2.2 , :

$$E_L\ ,\ E_R\ ,\ E_T\ ,\ \nu_{LR}\ ,\ \nu_{RT}\ ,\ \nu_{TL}\ ,\ G_{LR}\ ,\ G_{LT}\ ,\ G_{RT}$$

They are assembled in the buffer variable `parwm`. At the end of each loop cycle, the 9×12 - matrix `parwm` is stored in that cell of the three-dimensional cell array `par`, for which the position ⟨*row, column, page*⟩ correspond to the brick numbering specified by ⟨`brixx`, `briyy`, `briz`⟩.

In addition to the aforementioned mechanical parameters, other mechanical parameters (e.g. elasticity tensor $\mathbf{C}$ and Tsai Wu - parameters, which are not used in the simulation) are stored in the 9×12 - matrix `parwm`:

`parwm` =

⟨*elasticity-tensor* $\mathbf{C}$⟩ see Section 2.1 , Eq. (2.3) 6×6 - matrix									
$f_{yt,L}$	$f_{yt,R}$	$f_{yt,T}$	$f_{yc,L}$	$f_{yc,R}$	$f_{yc,T}$	f_{yLR}	f_{yLT}	f_{yRT}	
⟨12 Tsai Wu - *parameter*⟩									
E_L	E_R	E_T	ν_{LR}	ν_{RT}	ν_{TL}	G_{LR}	G_{LT}	G_{RT}	

Cracks are reproduced with cohesive elements. Damage initiation of cohesive elements refers to the beginning of disappearance of the cohesive element's stiffness. Damage initiation begins when the stresses satisfy the maximum nominal stress criterion. Therein, damage is assumed to initiate when the maximum nominal stress ratio reaches a value of one. This criterion can be represented as

$$\max\left\{\frac{\langle\sigma_i\rangle}{f_{yt,i}},\frac{\sigma_{ij}}{f_{y,ij}},\frac{\sigma_{ik}}{f_{y,ik}}\right\}=1\ ,\qquad i,j,k\ \in\ \{L,R,T\}\ . \tag{3.1}$$

The $\langle\,\rangle$ - brackets only take a non-zero value according to their argument in case of a positive stress σ_i. They are used to signify that a pure compressive stress state does not initiate damage. Strength values $f_{y\,t,\,L}$, $f_{y\,t,\,R}$, $f_{y\,t,\,T}$, $f_{y,\,LR}$, $f_{y,\,LT}$, $f_{y,\,RT}$ (Sec. 2.3) represent the peak values of the nominal stress at deformations either purely normal to the interface or purely in the first or the second shear direction, respectively.

The *Abaqus* output identifiers variable `MAXSCRT` indicates, whether the maximum nominal stress damage initiation criterion has been satisfied at a material point. The variable is disscussed by means of a sample plate in Section 4.4 .

To define the mechanical behavior of cohesive elements, a '*traction-separation*' approach is used [Abaqus Manual, 2009, 26.5.6 Defining the constitutive response of cohesive elements using a traction-separation description]. For example, the traction - separation description for the cohesive section on face 4 (detail of the cohesive element in Fig. 3.10, allocated to the global Y–Z - plane or local R–T - plane) requires three elastic constants and three strength values, related to the local R–T - plane:

$$\begin{aligned}&\text{Elastic constants} - E_L\,,\, G_{LR}\,,\, G_{LT}\ ,\\ &\text{strength values} - f_{y\,t,\,L}\,,\, f_{y\,LR}\,,\, f_{y\,LT}\ .\end{aligned}$$

Hence, to define three cohesive sections allocated to a brick, 18 parameters have to be extracted from the material parameter 9×12 - matrix of type `parwm` (Page 34) of the two adjacent solid bricks.

Listing 3.7: Mechanical parameter section 2

```
parcoh=cell(bripsi,bripsi,brilay)

for briz=1:brilay
  for briyy=1:bripsi
    for brixx=1:bripsi

% strength-parameter
parcohwm(2,1)=min(parwm{brixx,briyy,briz}...
  (7,1),parwm{brixx+1,briyy,briz}(7,1))
parcohwm(2,2)=min(parwm{brixx,briyy,briz}...
  (7,7),parwm{brixx+1,briyy,briz}(7,7))
```

```
% E, G - moduli
parcohwm(2,4)=min(parwm{brixx,briyy,briz}...
  (9,1),parwm{brixx+1,briyy,briz}(9,1))
parcohwm(2,5)=min(parwm{brixx,briyy,briz}...
  (9,7),parwm{brixx+1,briyy,briz}(9,7))

parcoh(brixx,briyy,briz)={parcohwm};  end;end;end
```

In Listing 3.7, the assignment of aforementioned mechanical parameters is described. Loops on brick level are used, to align the aforementioned mechanical parameters for cohesive elements. They are assembled in the buffer matrix `parcohwm`, wherein the six parameters stored in row 1 are required for material definition of the cohesive section on face 5, parameters in row 2 are required for cohesive section on face 4, and parameters in row 3 are required for the cohesive section on face 2. The function **`min`** is used, to filter the sought weakest parameters of adjacent solid bricks. For example, to define the strength value in L-direction (fiber direction) of the cohesive element detailed in 3.10, the smaller value $f_{yt,L}$ of both bricks with position ⟨`brixx`, `briyy`, `briz`⟩ and ⟨`brixx`$+1$, `briyy`, `briz`⟩ is taken, and stored in ⟨2,1⟩ of `parcohwm`.

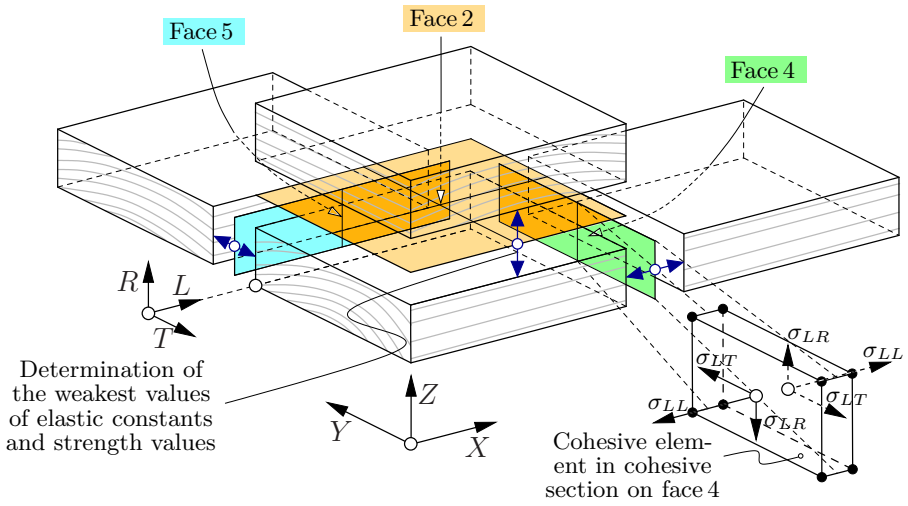

Figure 3.10: Read-out of strength values and elastic constants for the cohesive section

The mechanical parameters for the cohesive sections in `parcohwm` are stored similarly to the parameters for the solid section, in a three-dimensional cell array called `parcoh`, in which the matrices `parcohwm` for each element are included at the place

specified by the locations of the adjacent bricks.

$$\texttt{parcohwm} = \begin{bmatrix} f_{yt,T} & f_{y,LT} & f_{y,RT} & E_T & G_{LR} & G_{RT} \\ f_{yt,L} & f_{y,LR} & f_{y,LT} & E_L & G_{LT} & G_{LT} \\ f_{yt,R} & f_{y,LR} & f_{y,RT} & E_R & G_{LR} & G_{RT} \end{bmatrix}$$

3.4 Node and element - sets generating section

The surfaces of the solid and cohesive sections are tied together with mesh tie constraints according to [Abaqus Manual, 2009, 28.3.1 Mesh tie constraints]. To define surfaces, element sets containing all elements on brick surfaces are required. For example, elements with element numbers `1 01011 211` and `1 01011 221` in Fig. 3.5 are located on face 4 of brick number `1 01011`. To define all six surfaces of a solid brick with a variable mesh density, six element sets have to be defined: one for each face.

Listing 3.8: Element set generating section

```
elebr1=nodbr1(:,5)
elebr1=elesort(elebr1)

for briz=1:brilay
  for briyy=1:bripsi
    for brixx=1:bripsi

ibl(1)=ibl(1)+1

elebr=elebr1((1:elepbr)+((ibl(1)-1)*elepbr))
j=max(epbrxy^2,epbrxy*epbrz)*(ibl(1)-1)

% Elementset Face 4
j=max(epbrxy^2,epbrxy*epbrz)*(ibl(1)-1)
for i=1:epbrxy^2*epbrz
  if isface(elebr(i),7,epbrxy)
  j=j+1
  elefa1(j,4)=elebr(i)
  end
end;  end;end;end
```

`elebr1` contains all element numbers of the assembly, which are allocated to 20-node solid section elements. Again, loops on brick level (List. 3.8) are used to identify and sort elements of the current brick according to their position on exterior side faces. Here, `ibl(1)` is a counter on brick level needed to control the access to `elebr1`.

The subroutine `[logical]=isface(elenr,digit,location)` compares selectively digits (`digit`) of element numbers (`elenr`, $\langle l\ XXYYZ\ xyz \rangle$) with parameters indicating the element location in the brick (`location`). For example, brick number `1 01011` in Fig. 3.5 is investigated: to check, if one of the four elements, in the brick is located on exterior face 4 of the brick, the decisive digit 7 has to be compared with $\langle$*elements per brick in X - direction*$\rangle$ – `2` in this configuration. So, in this case digit 7 of element number `1 01011 211` has to be compared with value `2`. As output, logical *true* – 1, or *false* – 0 is displayed. For the example case, the result of `isface` is logical *true* – 1. The identified elements become part of the element set in column 1 of `elefa1`, which contains elements of all bricks, sorted by the location of elements in reference to exterior faces 1 to 6 . The side face number which elements are assigned to, is defined by the column number in `elefa1`:

`elefa1 =`

$\langle$*elements allocated to face 1*$\rangle$	$\langle$*elements allocated to face 2*$\rangle$	$\langle$*elements allocated to face 3*$\rangle$	$\langle$*elements allocated to face 4*$\rangle$	$\langle$*elements allocated to face 5*$\rangle$	$\langle$*elements allocated to face 6*$\rangle$	
						$\langle$*brick-no.*$\rangle$
						$\langle$*brick-no.*$\rangle$
⋮	⋮	⋮	⋮	⋮	⋮	

All other element and node sets are generated similarly to the aforementioned example, by filtering for decisive digit(s) of element and node numbers.

In Fig. 3.11 and Fig. 3.12, element and node sets generated in these section of the simulation program are presented. Figure 3.11 shows all cohesive sections as part of the model of the sample plate. While in Fig. 4.7 only cohesive sections of the bottom layer and on face 5 of the solid bricks are shown, herein also cohesive sections on face 4 and face 2 are depicted. Furthermore, the structure of the bottom layer, composed of parallel arranged boards, is apparent – for exemplification, every second board in the bottom layer is switched off. Board sets are stored in the data matrix `elslam`.

The node set for applying boundary conditions is apparent in Fig. 3.12 . For exemplification, the brick mismatch is set unequal to zero with `brimxy` and `brimz`.

Solid bricks with a mesh density of $\langle n.o.\ elements/solid\ brick \rangle = 8$ are shown. Node sets for boundary conditions are stored in `ndsbound`.

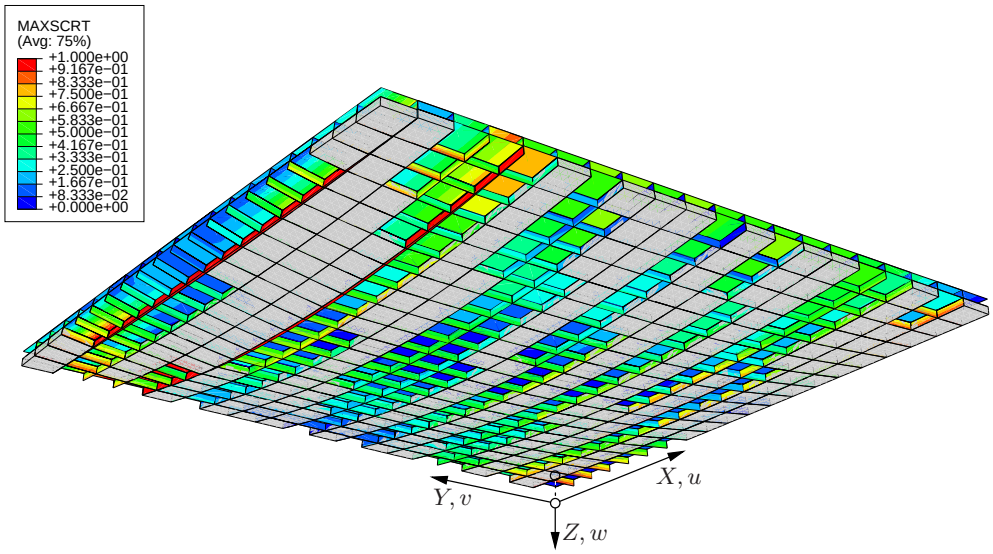

Figure 3.11: Cohesive grid, element set for boards

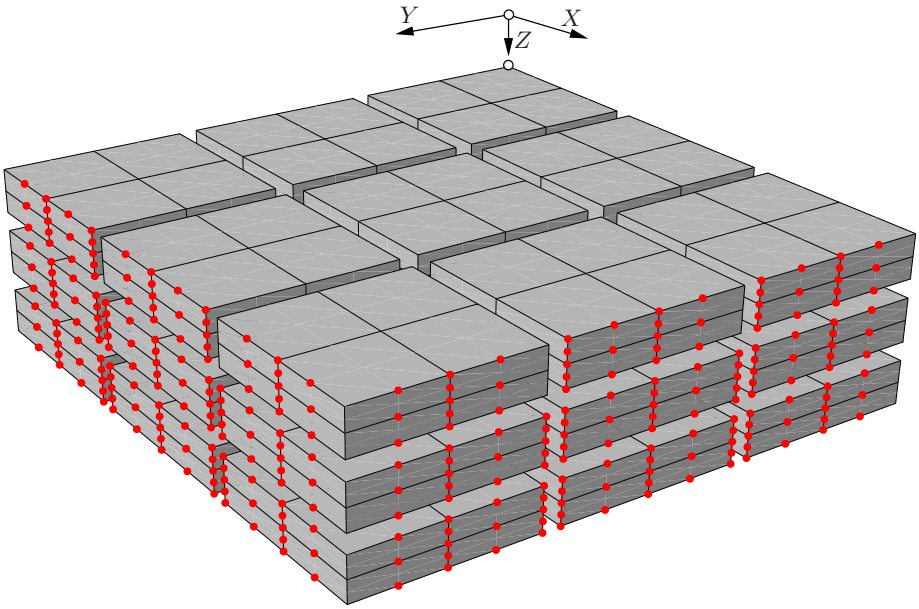

Figure 3.12: Node set for boundary

3.5 File generating section

In the closing section of the *Matlab* script file `inpgen.m`, the already generated data (Sec. 3.2 – 3.4) is reprocessed for printout to an *Abaqus* input-file, to be submitted to the solver *Abaqus/Standard*. A short summary of using input-files for *Abaqus* FE-calculation is done in Section 3.1 . Here, the main parts of this section are discussed.

The variable *job_name*, which specifies the name of the *Abaqus* input-file (*job_name*`.inp`), displays specification details of the generated FE-model of the CLT plate. Its syntax is

`b`⟨*n.o. bricks/side*⟩`_f`⟨*n.o. elements/solid brick*⟩`-`⟨*n.o. elements/cohesive sec. 5, 4*⟩`-`⟨*n.o. elements/cohesive section 2*⟩`_s5`⟨*running number of simulation*⟩`.inp` .

In List. 3.9 , the assembly of these file name is presented. Mesh density parameters `bripsi`, `elepbr`, `copfav` and `copfah`, which are introduced into the file name, have been in Section 3.2 . To generate the *job_name*, the **`sprintf`**-command is used, wherein the acronym '*n. o.*' stands for '*number of*'.

Listing 3.9: File generating section 1

```
filena=sprintf('inp/b%g_f%g-%g-%g_s%g.inp',...
  bripsi,elepbr,copfav,copfah, simn)
fid=fopen(filena,'w')

fprintf(fid,'*NODE\n**\n');
for i=1:size(cnodbr1,1)
  fprintf(fid,'%10d,%13.4f,%13.4f,%13.4f\n',...
  cnodbr1(i,1),cnodbr1(i,2),cnodbr1(i,3),...
  cnodbr1(i,4));
end
```

The file identifier `fid` is assigned by the command `fopen`, which creates a new file for writing with name *job_name*`.inp`. By access on `fid`, data is appended to the currently open input file. At first, the node definition (`*NODE`) for solid elements stored in `cnodbr1` is printed. To print data out of matrices, **`for`**-loops are used with a range controlled by the *number of rows*, the matrices are composed of; kind of process flow is used for all subsequent printout sections.

Listing 3.10: File generating section 2

```
fid=fopen(filena,'w')

for briz=1:brilay
  for brixx=1:bripsi
  for briyy=1:bripsi

fprintf(fid,'*ELEMENT, TYPE=C3D20\n');
  for ielem = 1:elepbr
    fprintf(fid,['%10u,%10u,%10u,%10u,'...
                 '%10u,%10u,%10u,%10u,'],...
      nodbr1((inl(1)-1)*20*elepbr+20*ielem-19,5)

fprintf(fid,'*ELSET, ELSET=BRICK-1%05u,...
  INTERNAL\n',brinr)
for i=1:elepbr
  elenr=nodbr1((inl(1)-1)*20*elepbr+20*i-19,5)
  fprintf(fid,'%9u',elenr); end

fprintf(fid,['*SOLID SECTION,'...
  'ELSET=BRICK-1%05u,ORIENTATION=LAYER-1,'...
  'MATERIAL=M%05u\n'],brinr,brinr); end;end;end

fprintf(fid,['*ORIENTATION,NAME=LAYER-1\n'...
             ' 1, 0, 0,  0, 0, 1\n 1,0\n'...
             '*ORIENTATION,NAME=LAYER-2\n'...
             ' 1, 0, 0,  0, 0, 1\n 2,90\n']);
```

Like in aforementioned sections, loop cycles on brick level are used to write out data concerning brick definition (List. 3.10). In these cycles, the following keywords are defined: `*ELEMENT`- definition of element connectivity based on node numbers; `*ELSET` – definition of element sets for material section assignment (Sec. 3.3), element sets for surface definitions (`elefa`⟨*no.*⟩ in Sec. 3.4); `*SURFACE`- definition of surfaces on brick level; `*SOLID SECTION` and `*COHESIVE SECTION` definition of sections for material specifications. For keyword definition details, see [Abaqus Manual, 2009, Abaqus Keywords Reference Manual]. For a specification of data matrices used for printout in this section, see Tab. 3.1 .

For example, to define the eight solid elements allocated to the current brick in Fig. 3.6 , the `for`- loop requires eight cycles according to the number of elements per brick (`elenr`) to readout element definition data from `nodbr1` (detailed on Page 27).

In the section definition, the principal material directions for each brick are defined. For bricks in layer 1, orientations according to the direction of the lamellae in the exterior layer 1 and layer 3 are assigned. The same procedure applies for bricks in layer 2. The definition of the orientation is done after the loop cycles on brick level with keyword `*ORIENTATION`.

Listing 3.11: File generating section 3

```
fprintf(fid,'*NSET,NSET=BOUND-13-0')
for i=1:size(ndsbound,1)
  nodnr=ndsbound(i,1)
  fprintf(fid,' %9u',nodnr); end

fprintf(fid,['*TIE,NAME=%05u-5,ADJUST=NO,...
  'TYPE=SURFACE TO SURFACE\n'...
  'I.SURFACE-1%05u-3,I.SURFACE-1%05u-5\n'],...
  brinr,brinr+10,brinr)

for briz=1:brilay
  for brixx=1:bripsi
  for briyy=1:bripsi

fprintf(fid,['*MATERIAL,NAME=M%05u\n*ELASTIC',...
  'TYPE=ENGINEERING CONSTANTS\n'...
  '%8.2f,%7.2f,%7.2f,%8.6f,%8.6f,%8.6f,'...
  '%7.2f,%7.2f\n%8.2f\n'],brinr,...
  par{brixx,briyy,briz}(9,1),...
```

A exemplarily printout conditions of a node set needed for specification of boundary conditions is depicted in List.3.11. Node sets for boundary are stored in `ndsbound`; In column 1 of (`ndsbound(i,1)`), all nodes located at the lateral face with attribute $x = 0$ are stored. They are printed out in a node set called `NSET=BOUND-13-0`.

To «tie» surfaces of sections of the FE assembly with each other, the `*TIE`-keyword is used according [Abaqus Manual, 2009, 28.3.1 Mesh tie constraints].

To printout material definition, the mechanical parameters stored in `par` (Section 3.3) are required. Due to the data type of `par` (three dimensional cell array), the access is again made to by loop cycles on brick level. In the example, engineering constants (nine elastic parameter) are printed out of row 9 of the 9×12 - matrix `parwm` (Page 34), which is located at a position corresponding to the current brick controlled by $\langle brixx, briyy, briz \rangle$.

Table 3.1: Data matrices used for printout

`nodbr1 nodbr5` `nodbr4 nodbr2`	Node number data matrices containing nodal coordinates, as well as the allocation ot the nodes to elements (`nodbr1` – solids, `nodbr`⟨*no.*⟩ – cohesives). For the layout of the variables `nodbr1`, `nodbr4` – see Pages 27 and 29 in Section 3.2 . Used for element definition with keyword `*ELEMENT` .
`cnodbr1 cnodbr5` `cnodbr4 cnodbr2`	Node numbers with nodal coordinates without multiple node definitions like in `nodbr`⟨*no.*⟩ No element numbers assigned. Used for node definition with keyword `*NODE` .
`par parcoh`	Three dimensional cell array storing material parameters. Parameters for solid bricks are stored in cells of `par`, with format of type `parwm` – see Page 34 . Strength values and elastic constants for cohesive elements are stored in cells of `parcoh`, with format of type `parcohwm` – see Page 37 .
`ndsbound`	Node sets for boundary conditions; four sets in columns 1 – 4, one for each lateral face according to Fig. 3.1 .
`elefa1 elefa5` `elefa4 elefa2`	Element sets for surface definition of bricks see Section 3.4; `elefa1` (see Page 38) . The surface definition variable for solid brick elements contains six columns of element sets according to the hexahedron shape with six side faces. Element sets in `elefa`⟨*no.*⟩ are required for the surface definition of the cohesive sections. They contain two columns of element sets for surface definition, due to the composition of cohesive elements of two faces.
`elslam`	Contains element sets of solid elements, assigned to boards with randomly distributed lengths, respectively. Boards are sections of which the endless lamella is built (Section 2.5).

Chapter 4

FEM-calculation, discussion

In this chapter, results of the FE calculations of CLT plates, built-up with the simulation program presented in Chapter 3 , are discussed.

Due to convergence problems in the FE analysis, at progressive fracture in cohesive layers, ultimate failure loads were not determined. Rather, a qualitative discussion of results of the FE calculation has been made. Furthermore, node and element sets generated with the simulation program are displayed in figures in order to present the features of the model.

4.1 Plate geometry, applied load, and boundary of the sample plate

The mechanical behavior of CLT plates discussed in below sections is based on calculations of a sample plate displayed in Fig. 4.1 .

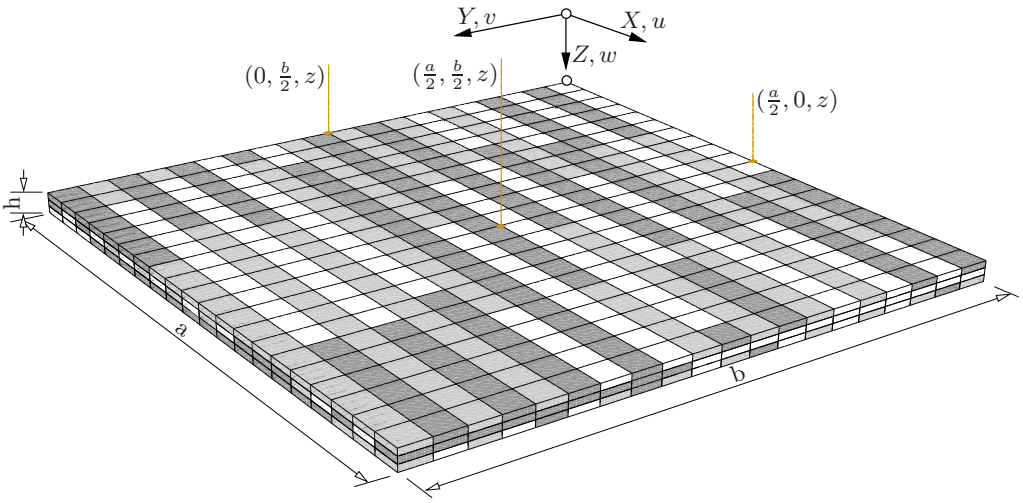

Figure 4.1: Sample CLT plate

As specified in Section 3.2, the lateral length ($a = b$) of the quadratic sample plate (Fig. 4.1) is controlled by the numbers of parallel arranged 'lamella sections'. The dimensions of the endless lamella, of which the CLT plate is composed, are set according to Fig. 2.6 in Section 2.5 with $\langle width \rangle = 150\,\text{mm}$ and $\langle height \rangle = 35\,\text{mm}$. As apparent in the figure, the example plate is built-up of 20 'lamella sections' per side, which results in a lateral plate length of $a = b = 3000\,\text{mm}$. The example plate with three layers has a total thickness of $h = 105\,\text{mm}$. The plate is generated with distribution parameters, 'length of boards', 'density ρ', and 'KAR - value', according to Subsections 2.5.1 – 2.5.1 . The unequal lengths of the boards (as subparts of the endless lamella) are apparent in Fig. 4.1 .

The sample plate used for the studies is subjected to a distributed load according to Fig. 3.2 . The sample plate is simply supported (Fig. 3.1) as specified in detail on Page 19 .

The simulating process used for the plate, is load controlled. Due to the aforementioned convergence problems, the load level set for the sample plate (0.2 N/mm^2) could not be reached. All investigations of the stress and displacement states in below paragraphs, are made on a load level of about 52 % of the aforementioned distributed load. It is the load level for the current plate configuration (geometry, mesh density, technological parameters), at which convergence problems occur.

In the following study, distributions of stresses through the plate thickness as well as displacement components are investigated on selected positions of the CLT plate.

4.2 Cross-sectional warping and stress distributions of CLT

The laminate specific, zig-zag shaped course of the in-plane displacement across the plate thickness is studied on the sample plate discussed in Section 4.1 , Fig. 4.1 . Figure 4.2 depicts the characteristic courses of u and v across the thickness, at the position (marked in Fig. 4.1), where they assume their maximum values: u at $(0, \frac{b}{2}, z)$ and v at $(\frac{a}{2}, 0, z)$. The zig-zag shape of the displacement u is most obvious. It results from the high shear deformations in the middle layer in consequence of the high stiffness contrast in X - direction of the two exterior layers and the interior layer, in combination with the very low shear modulus G_{RT} of the latter in the X–Z - plane. Regarding the displacement v, there is almost no zig-zag pattern observed. The middle layer exhibits high bending stiffness in the Y - direction, so that the soft surface layers just follow the displacement predominately enforced by the middle layer Stürzenbecher [2010].

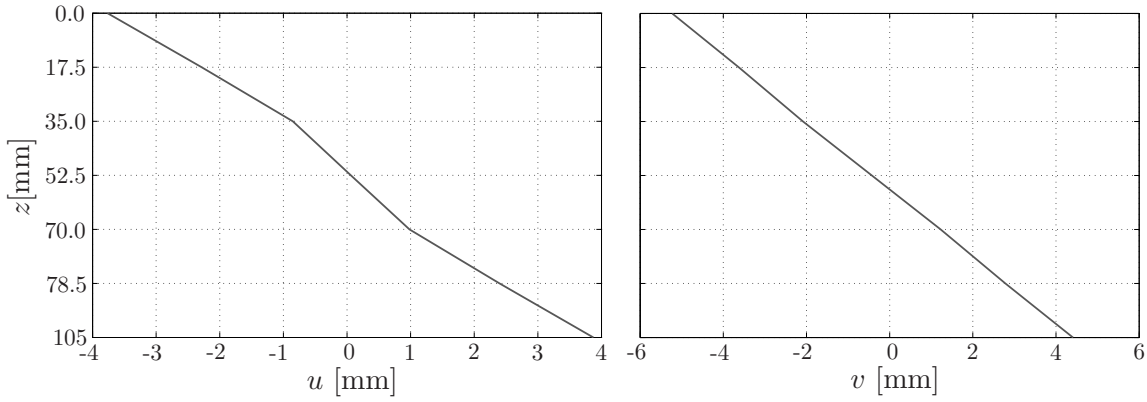

Figure 4.2: Displacement course through the plate thickness;
u at $(0, \frac{b}{2}, z)$ and v at $(\frac{a}{2}, 0, z)$

Element based results like stresses, subscripted with x, y, z, are applied to the global $X-Y-Z$ directions of the coordinate system shown in Fig. 4.1 , as in all subsequent figures. In Fig. 4.3 the two in-plane stress components σ_{xx} and σ_{yy} are presented. They exhibit the correct characteristic shape, namely discontinuities at the layer boundaries and considerably different slopes in soft and stiff layers. The in-plane shear stresses τ_{zx} and τ_{zy} are presented in Fig. 4.4.

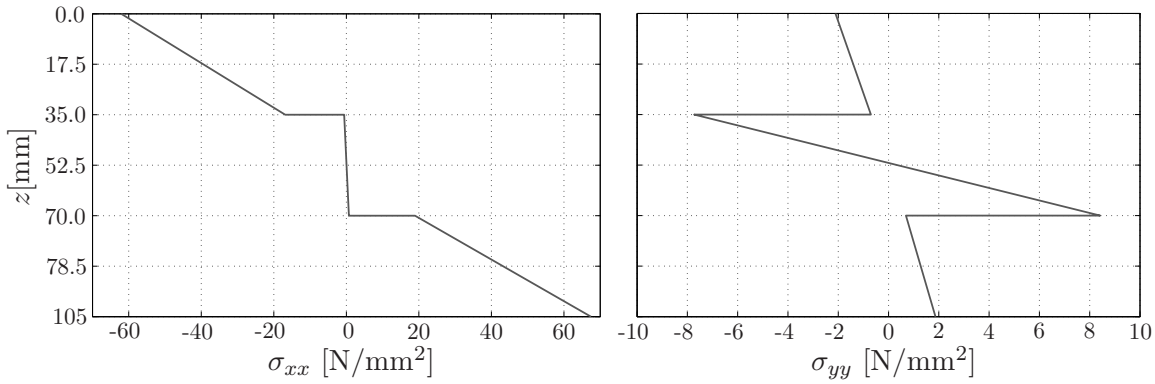

Figure 4.3: Course of stresses σ_{xx}, σ_{yy} through the plate thickness at $(\frac{a}{2}, \frac{b}{2}, z)$

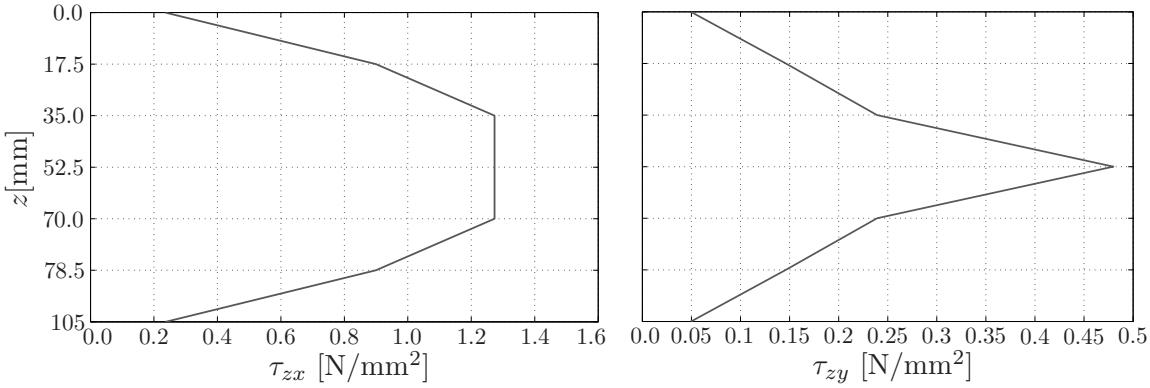

Figure 4.4: Course of shear stresses through the plate thickness; τ_{zx} at $(0, \frac{b}{2}, z)$ and τ_{zy} at $(\frac{a}{2}, 0, z)$

4.3 Force - displacment relation, crack initiation

As mentioned in Section 4.1, convergence problems of the FEM solver occurs during the formation of cracks in the bottom surface layer ($z = h$), which is subject to tension stresses. In Fig. 4.5, the force-displacement curve at the plate's center point $(\frac{a}{2}, \frac{b}{2}, h)$ is plotted. The ordinate of the diagram is labeled with 'Reaction force', as the sum of bearing forces acting at constraint nodes (red nodes in Fig. 3.12). In load controlled non-linear simulation procedures, the load is applied in steps. In the load curve in Fig. 4.5, steps are marked with 'cross' - symbols. The first crack occurs at step number eight (marked). From there on, the increment-size is more and more reduced by the solver-algorithm of *Abaqus*. The depicted load curve exhibits 38 steps; at step 38 the numerical calculation process is stopped manually.

The force-displacement diagram shows the characteristic linear elastic material behavior of the plate until the first crack occurs at step eight (Fig. 4.5). Despite the initiating crack process and the local mechanical failure in according to the model 'ideal elastic - fracture' presented in Fig. 2.7 , the mechanical characteristic of the system 'CLT plate' remains almost linear at the global scala until the abort at step 38. To visualize the initiating crack process, model plots of the sample plate are discussed below in Section 4.4 .

A global linear mechanical characteristic was also observed in tests on CLT plates with a similar test setup, carried out by MPA Stuttgart on behalf of IMWS in spring 2011.

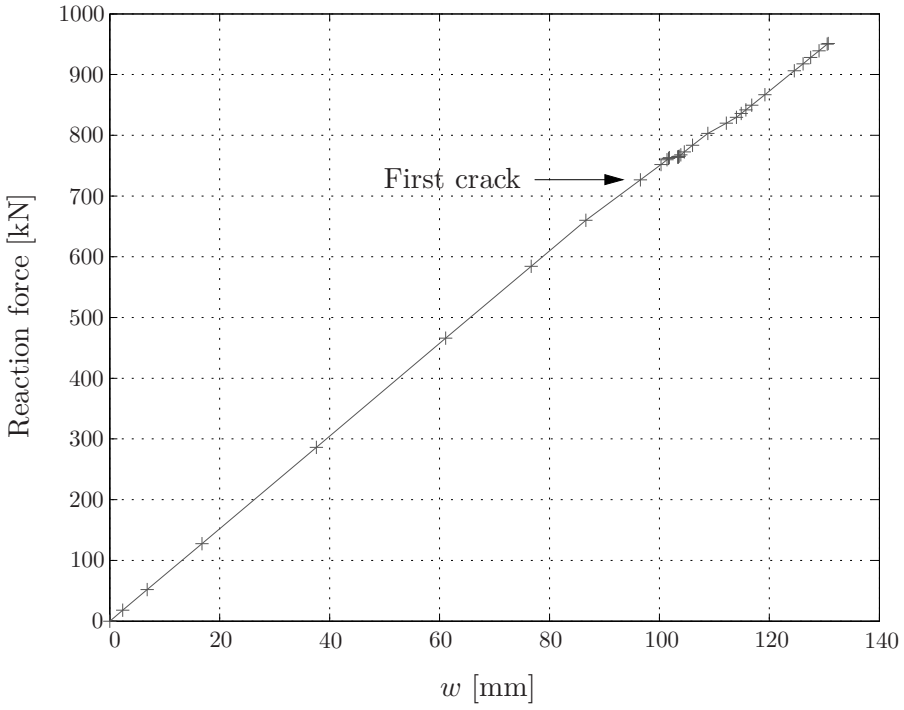

Figure 4.5: Displacement w at plate center point $(\frac{a}{2}, \frac{b}{2}, h)$

4.4 Crack formation – influence on the distribution of stress

In Sections 4.2 – 4.3, the distribution of stresses through the plate thickness as well as the load-displacement curve over time at the plate's center point were presented. The results of these studies, coincide with the investigations on plates with elastic material behavior done by Radecki [Radecki-Pawlik, 2009, Chapter 6].

In the current section, special issues concerning the specific built-up of generated CLT plates are discussed. Furthermore, the mechanical behavior concerning the formation of cracks in the performed calculation of the sample plate are presented: the characteristic normal stress distribution in global X - direction (local L - direction in surface layers); the displacement field in Z - direction of the cracked sample plate; the state of the fracture formation in the cohesive sections of the bottom layer, specified by a variable indicating the damage initiation criterion.

The mesh density of the solid section used for the calculation of the sample plate is apparent in Fig. 4.7 . In the remaining figures, only edges of «sections» according

to the definition in Section 3.1 are plotted.

Indices $\langle 1,\ 2,\ 3 \rangle$ used by *Abaqus* and appearing in the figures correspond to $X-Y-Z$ denoting the directions of the global coordinate system used in this work.

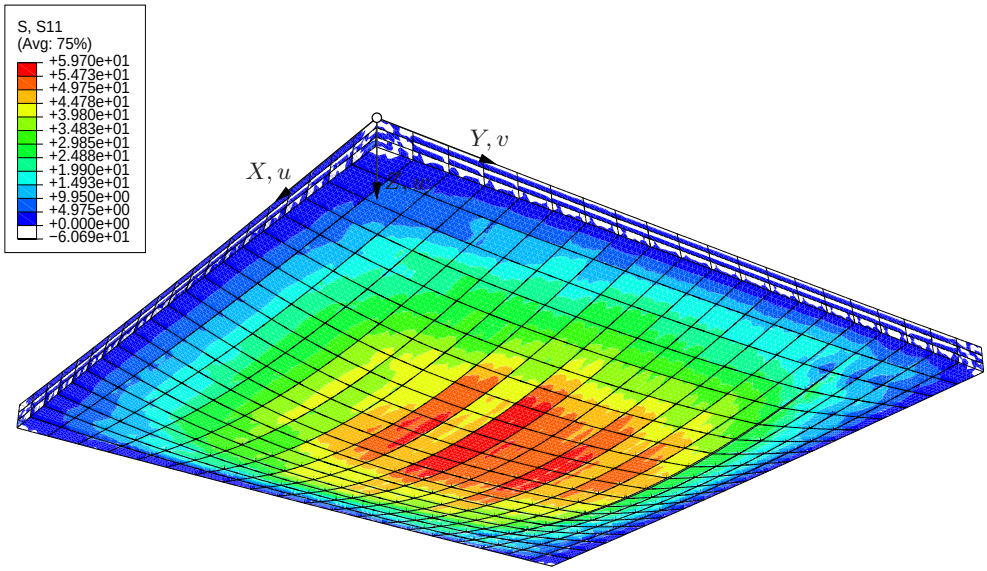

Figure 4.6: Distribution of stress component σ_{xx} [N/mm^2] at the bottom surface

In Fig. 4.6, the stress component in fiber direction, σ_{xx} , of the bottom layer is plotted. As apparent, the amplitude of the stress state depends on the material parameter of each lamella section. The high stiffness contrast of the parallel arranged lamella sections is apparent through the different sizes of the tension stress components σ_{xx} in these sections. Soft lamella sections just follow stiffer lamella sections exhibiting a higher specific higher YOUNG's modulus E_L.

The variable `MAXSCRT` plotted in Fig. 3.11 indicates whether the maximum nominal stress damage initiation criterion (Equation 3.1) has been satisfied. The margin of `MAXSCRT` rages from 0 to 1, where a value of 1 indicates that the initiation criterion has been met [Abaqus Manual, 2009, 29.5.6 Defining the constitutive response of cohesive elements using a traction-separation description].

Hence, in red colored cohesive layers (Fig. 3.11) the criterion has been satisfied and a crack has occurred. Whether it is open, depends on the quality of the strain state for which the damage initiation criterion has been met, namely if strains occurred in purely normal directions or purely in the first or the second shear direction.

In calculations of several plates with varying geometries and properly assignment

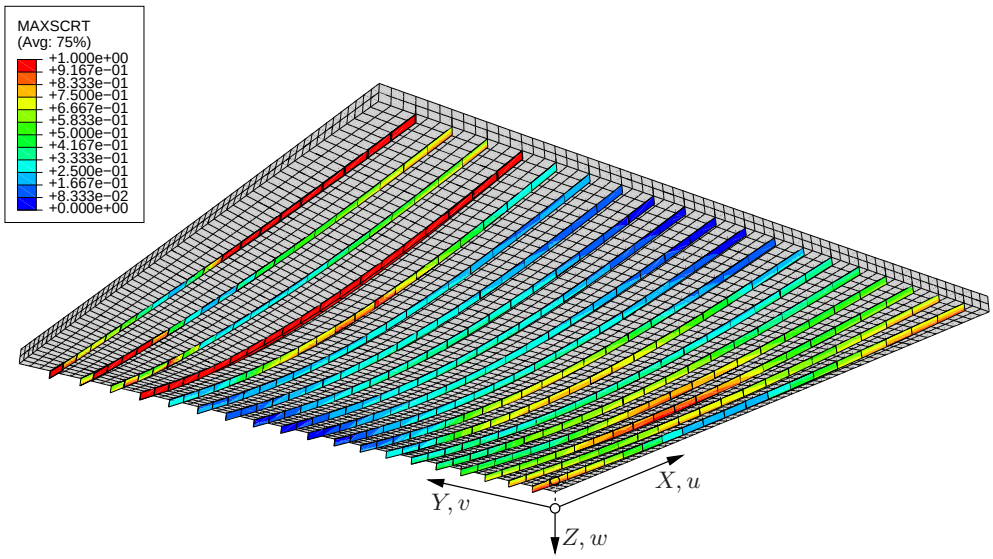

Figure 4.7: Cohesive layers in between lamella sections in L - direction; `MAXSCRT` - criterion; meshed solid section

to the sections, generated by the *Matlab*-simulation program (Chap. 3), the formation of cracks always occurs first in cohesive layers arranged in between the parallel arranged lamella sections, as it is the case for the sample plate shown in Fig. 3.11. . Hence, it is obvious that these cracks those are allways located next to the line support of the CLT plate, occured due to the breakdown of cohesive elements initiated by shear stresses those are matching the maximum nominal stress criterion.

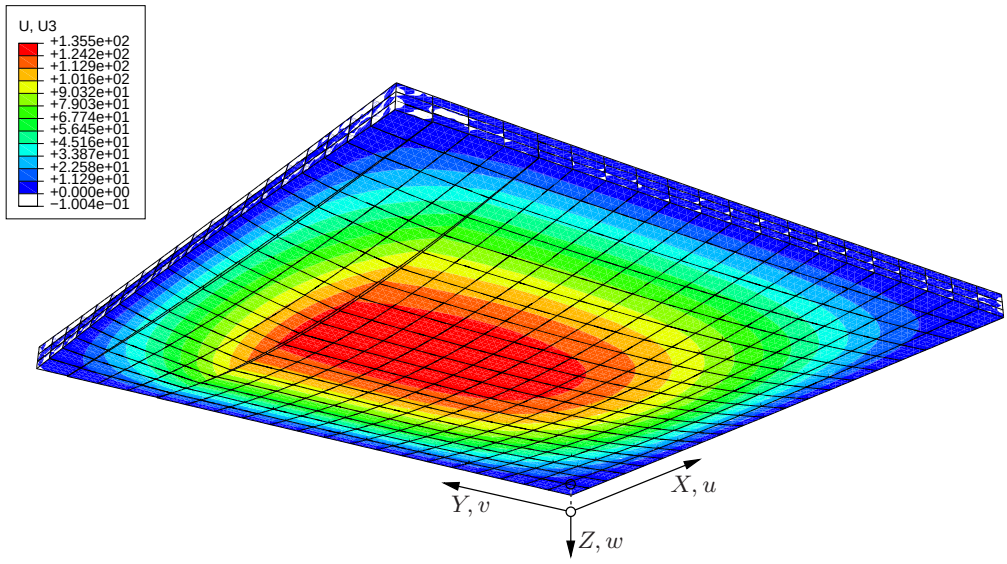

Figure 4.8: Distribution of deflections w [mm], at the bottom surface

Fig. 4.8 shows the distribution of deflections of the plate's bottom face in Z-direction. The asymmetrical displacement field results from two cracks in the field along the line support at (x, b, h). The two cracks in between the 15th and the 16th lamella section aligned in X-direction, as well as in between the 19th and the 20th section, are apparent as double lines at the bottom surface.

Chapter 5

Conclusions

5.1 Summary

This thesis deals with the development of a simulation tool for the investigation of the mechanical behavior of early stages of brittle failure in quadratic 3-layer CLT plates under distributed load. The main focus was to create a FE model for these plates, including a fracture mechanical approach for wood under tensile load, in which the mesh density and material sections can be flexibly defined. This approach enables to compare simulation plates modeled with almost similar material parameters obtained for different mesh densities. To build up the individual layers in the model of CLT, an 'endless lamella' was defined, where variable lengths, densities, and knot contents of boards are taken into consideration. To assign the mentioned technological parameters to parts of the CLT plate (the endless lamella, respectively) was divided into sections of 'bricks' and 'boards'. Mechanical parameters of wood (elastic constants and strength values) are calculated on basis of a micromechanical model, as functions of the technological parameters density ρ, knot content of boards KAR, and moisture content u. The assembly as foundation of the modeling process, as well as the data flow of the simulation program were detailed and explained by examples.

In the last section, an example calculation of a plate generated by the simulation program was shown. The high shear compliance of CLT due to its cross-wise lay-up and the highly anisotropic behavior of its constitutive layers was discussed on basis of the computation results. To investigate the mechanical behavior of the plate during the crack formation, a load-displacement curve was presented. A general pattern of cracking was observed in the calculations of several plates with randomly generated geometries and material paramter assignments, namely that the initial formation of cracks occurs in cohesive layers arranged in longitudinal direction next to the line support as shown in Fig. 4.7 . For the load-displacement curve, also different plates showed the same hand of an almost linear mechanical characteristic during the crack formation process.

5.2 Perspective

The structured layout of the specific program sections (see flowchart on Fig. 3.4) enables a relatively easy enhancement of the ability of the simulation program presented in this thesis. The mesh generating section as core of the simulation program, with its characteristic node and element numbering scheme, allows to define different geometries by a straightforward adaptation of the program code. For example, an extension of the mesh generating section in order to generate arbitrary multilayer non-quadratic CLT plates (e. g. CLT elements with three, four, five layers) is possible with a reasonable effort. Furthermore, the implementation of cut-out areas is feasible, if their dimensions coincide with the lamella-width increment. But it is essential, to stick to the assembly of rectangularly arranged 'brick'-sections as units for material parameter assignment. The distinctive node and element numbering syntax enables an easy definition of additional surface, node, or edge sets to apply various types of loading as well as boundary conditions. The plastic material model (suitably described through the Tsai-Wu failure criterion) for onset for plastification in the compressive zone of CLT is not fully integrated yet, but could easily be added.

With the developed subroutines, containing a controllable random stream selection switch for distribution parameters, the stochastic analysis of investigated plates is possible.

Bibliography

[Abaqus Manual, 2009] Dassault Systemes: *Abaqus User's Manual.* Version 6.9-EF, 2009.

[Blaß et al. , 1995] Blass, J. ; Görlacher, R. ; Steck, G. : *STEP 1, Holzbauwerke nach Eurocode 5, Bemessung und Baustoffe.* Düsseldorf: Selbstverlag, 1995.

[Eberhardsteiner, 2002] Eberhardsteiner, J.: *Mechanisches Verhalten von Fichtenholz.* Springer Wien New York, 2002. – ISBN 3-211-83763-9 .

[Ehlbeck et al. , 1985] Ehlbeck, J. ; Colling, F. ; R.Görlacher: Einfluß keilgezinkter Lamellen auf die Biegefestigkeit von Brettschichtholzträgern. In: *Holz als Roh- und Werkstoff* 43, 1985, S. 333–337, 369–373, 439–442 .

[Fleischmann, 2005] Fleischmann, M.: *Numerische Berechnung von Holzkonstruktionen unter Verwendung eines realitätsnahen orthotropen elasto-plastischen Werktstoffmodells*, Technische Universität Wien, Doctoral Thesis, 2005.

[Henze, 2008] Henze, N.: *Stochastik für Einsteiger.* Vieweg & Sohn, 2008. – ISBN 978-3-8348-0423-5 .

[Kühne, 1955] Kühne, H.: Über den Einfluss von Wassergehalt, Raumgewicht, Faserstellung und Jahrringstellung auf die Festigkeit und Verformbarkeit schweizerischen Fichten-, Tannen-, Lärchen-, Rotbuchen- und Eichenholzes. In: *EMPA-Bericht* 183, 1955.

[Mang & Hofstetter, 2000] Mang, H. ; Hofstetter, G.: *Festigkeitslehre.* Springer Wien New York, 2000. – ISBN 3-211-83419-2 .

[Matlab Documentation, 2009] Math Works: *Matlab Documentation.* Version R2009a, 2009.

[Pagano 1970], Pagano, N.: Exact solutions for rectangular bidirectional composites and sandwich plates. In: *Journal of Composite Materials* 4 , 1970, S. 20–34 .

[Radecki-Pawlik, 2009] Radecki-Pawlik, B.: *Numerical simulation of the load bearing behavior of cross-laminated timber*, Technische Universität Wien, Diploma Thesis, 2009.

[Studiengemeinschaft Holzleimbau e.V.] Studiengemeinschaft Holzleimbau e.V.: *Brettsperrholz (BSP)*. `http://www.brettsperrholz.org/publish/93fe150d_e081_515d_740d66c560e0e6bd.cfm?m_id=6`, – retrieved 18-March-2011.

[Stürzenbecher, 2010] Stürzenbecher, R.: *Mechanical behavior of engineered wood products: Experimental investigation and advanced modeling of Veneer Strand Boards and Cross Laminated Timber*, Technische Universität Wien, Doctoral Thesis, 2010.